APPLICATION OF MODIFIED LOG-WAKE LAW IN NONZERO-PRESSURE-GRADIENT TURBULENT BOUNDARY LAYERS

MA QIAN

NATIONAL UNIVERSITY OF SINGAPORE

2004

APPLICATION OF MODIFIED LOG-WAKE LAW IN NONZERO-PRESSURE-GRADIENT TURBULENT BOUNDARY LAYERS

MA QIAN

(*M. Eng., Tsinghua*)

A THESIS SUBMITTED

FOR THE DEGREE OF MASTER OF ENGINEERING

DEPARTMENT OF CIVL ENGINEERING

NATIONAL UNIVERSITY OF SINGAPORE

2004

ACKNOWLEDGEMENT

I would like to take this opportunity to express my sincere gratitude and appreciation to my supervisor Dr. Guo Junke, John and co-supervisor Dr. Cheng Ming for their keen guidance, encouragement, invaluable advice and endless support during the course of this work. I am highly indebted to my supervisors for their personal care and affection and for making my stay in Singapore a memorable experience.

I am thankful for the financial support of a research scholarship provided by the Institute of High Performance Computing. Additionally, I would like to give my appreciation to the staff of the Hydraulics Laboratory for their technical assistance and to my colleagues for their advice and support.

I also owe gratitude to the thesis examiners for their helpful suggestions to improve the thesis.

Last but not least, I would like to express my gratitude to my wife Li Yan for her steadfast support and encouragement.

TABLE OF CONTENTS

SUMMARY

The velocity distribution of boundary layers plays an important role in modern fluid mechanics and hydraulics. The logarithmic law and log-wake law are widely used to describe the velocity distribution. They, however, does not work for near the wall and near the boundary layer edge since it does not satisfy the zero velocity gradient requirement at the boundary layer edge.

Recently, Guo et al. (2003) proposed a modified log-wake law (MLWL) to simulate the velocity profile of turbulent zero-pressure-gradient flat plate boundary layers, which improved the conventional log-wake law by meeting the zero velocity gradient requirement at the boundary layer edge. In this thesis, the MLWL is extended to simulate the velocity distribution of turbulent nonzero-pressure-gradient flat plate boundary layers. It is shown that pressure gradient only affects the wake strength in the modified log-wake law while all other parameters keep the same as those in zero-pressure-gradient flows.

Specifically, the MLWL was validated by comparing with eight high quality experimental data sets in pressure gradient (both favorable and adverse pressure gradient) domains. The comparison shows the basic structure of the MLWL is correct and it is suitable not only to simulate the velocity profiles but also to predict the skin friction factor of turbulent flat plate boundary layers. A new correlation of Coles' wake strength Π with Clauser pressure gradient parameter β is constructed in this thesis.

On the other hand, the open-channel flow has the same form of governing equation as the flat plate boundary layer. The log law and the log-wake law are then also widely employed to open-channel flows. Again, the conventional models do not meet the upper boundary condition. In particular, the conventional models cannot reflect this phenomenon in open channels.

Numerical experiments are conducted to identify whether the MLWL is or not suitable to simulate gradually varied open-channel flows (2D), like flow entering reservoirs. The comparison of the MLWL with the numerical experimental data shows the MLWL agrees with the numerical data excellently and the MLWL can reflect the velocity dip phenomenon very well. Besides a relationship of Coles' wake strength Π with pressure gradient parameter β_p are presented in this thesis.

In brief, this study shows that the MLWL can simulate the velocity distribution of turbulent flows over flat plates and in open channels with pressure gradient.

LIST OF SYMBOLS

The following symbols are used in this paper:

Notation

a, b, c	Constants in the power law (3.17)
B	Additive constant in the logarithmic law (2.1)
B_1	Additive constant in the friction equation (3.44), (3.63)
c	Sound speed
c_f	Skin friction factor
D_h	Hydraulic diameter of square tube
F, f, f_1	Functional symbols
Fr	Froude number, $U/\sqrt{gh}$
g	Gravitational acceleration
h	Flow depth of open channel
K	Acceleration parameter in (4.3)
P	Functional symbol
p	Pressure
p^*	Total pressure head of open-channel flow
q	Dscharge per unit width
R_h	Hydraulic radius

R_{e_δ} Reynolds number based on the boundary layer thickness, $\delta u_* / \nu$

R_{e_θ} Reynolds number based on the momentum thickness, $\theta U/\nu$

S Channel bottom slope

U Freestream velocity of boundary layer or mean (depth-averaged) velocity of open-channel flow

u Time-averaged velocity in the downstream direction

$u_{\max}$ Maximum velocity in the flow direction

u_* Wall shear velocity

u' Fluctuating velocity component in x direction

V Transverse velocity at the boundary layer edge

v Time-averaged velocity normal to the wall

v' Fluctuating velocity component in y direction

W Wake function

$W(\xi)$ Wake function

w Open-channel width

x Coordinate of the downstream direction

y Coordinate of the lateral direction in 3D or normal to the wall in 2D problem

z Coordinate of the upward direction that is perpendicular to x-y plane

y^+ Inner variable, yu_* / ν

Greek symbols

α Constants in the friction equation (3.63)

β Clauser pressure gradient parameter, $\beta = \left(\delta^* / \rho u_*^2\right)\left(\partial p / \partial x\right)$ for boundary layer, $\beta = \left(\delta^* / \rho u_*^2\right)\left(\partial p^* / \partial x\right)$ for open-channel flow

β_h Pressure gradient parameter for open-channel flow, $\left(h / \rho u_*^2\right)\left(\partial p^* / \partial x\right)$

β_p New pressure gradient parameter for open-channel flow, $\left(h / \rho u_*^2\right)\left(\partial p / \partial x\right)$

δ Boundary layer thickness

δ^* Boundary layer displacement thickness

θ Boundary layer momentum thickness

η Transverse velocity distribution function

κ Von Karman constant in the logarithmic law

κ_1 Von Karman constant in the friction law (3.44)

μ Fluid viscocity

ν Kinematic viscosity of fluid

ν_t Kinematic eddy viscosity

ξ Relative distance from the wall, y/δ

Π Coles wake strength

Π_0 Coles wake strength of ZPG boundary layer

Π_p Coles wake strength directly reflects the effects of pressure gradient

ρ Fluid density

σ Water-air surface tension

τ Local shear stress

τ_t Turbulent shear stress

τ_v Viscous shear stress

τ_w Wall shear stress

χ Proportional constant in the transverse velocity function

ζ Constants in the friction equation (3.63)

LIST OF FIGURES

LIST OF TABLES

CHAPTER ONE

INTRODUCTION

1.1 BACKGROUND

Since Prandtl conceived of the idea of the boundary layer in 1904, the boundary-layer theory has developed for a century and stands the test of time.

The velocity distribution of boundary layers is a basic subject for boundary layer related problems. Once the velocity profile is obtained, other variables, such as flowrate, shear stress, wall shear velocity, skin-friction factor, etc., can be calculated. Phenomena such as particle transport, diffusion, erosion and deposition or flow resistance, which are of importance to the hydraulic engineer, are linked with the velocity characteristics. How to get the proper velocity profile is the key for applying boundary layer theory accurately from both the theoretical and practical points of views.

Despite the fact that the boundary layer of a flat plate is the simplest situation and has been studied for a century, the velocity profile formula does not exactly compare to experiment data.

Normally, the velocity profile of a flat plate boundary layer is described in power law or logarithmic law, both of these two forms fit the experimental data well except for near the wall and near the boundary layer edge since it does not satisfy the edge condition $du/dy = 0$ at $y = \delta$, and the physical significance of each term in the law can not be interpreted clearly.

Recently, Guo et al. (2003) proposed a modified log-wake law (MLWL) to simulate the velocity profiles of turbulent zero-pressure-gradient (ZPG) flat plate boundary layers, which improves the conventional log-wake law by meeting the zero velocity gradient requirement at the boundary layer edge. Comparison of Guo's equation with corresponding experimental data showed this equation does work fairly well, and each term in Guo's equation iss reasonably interpreted in clear physical meaning. Another interesting thing is that some parameters in Guo's equation are universal constants.

The studies on turbulent nonzero-pressure-gradient (NPG) flat plate boundary layers which may separate from the wall are more practically important than these on ZPG boundary layers. The same problem to meet the zero velocity gradient requirement also exists in the NPG boundary layers. Similarly, it is reasonable to consider cracking such problems by applying the MLWL to the turbulent NPG flat plate boundary layer flows.

On the other hand, the log law and log-wake law have been employed to describe the velocity profile of open-channel flow since Keulegan (1938) suggested the logarithmic

velocity distribution to hold the entire depth of open-channel flow. Lemmin and Rolland (1997) reported that the velocity dip may also occur in natural wide channels at large width-depth ratios, e.g., w/h = 20 ~ 40, where w is the width of channel, h the depth of water. That means the requirement of meeting the zero velocity gradient at the maximum velocity also should be satisfied. Obviously, the log-wake law cannot meet this requirement. Again, the MLWL is employed to deal with the same question and study the characteristics of uniform and non-uniform open channel flows. Actually, another important advantage of MLWL is that it can replicate the velocity dip phenomenon in open channels, i.e., it can not only describe the velocity profile below where the maximum velocity occurs but also continuously simulate the velocity profile above the maximum velocity till the free surface.

1.2 SCOPE OF STUDY

Actually, Guo's equation for turbulent flat plate boundary layers is proposed for the zero-pressure-gradient flat plate boundary layer flows. Could it be applied for the turbulent nonzero-pressure-gradient flat plate boundary layer flows?

My research work in this thesis is to answer this question. The whole thesis focuses on two aspects, i.e.

a) Whether the structure of MLWL equation is suited or not for turbulent NPG flat plate boundary layers?

b) When the applicability is validated, how to determine the corresponding parameters involved in this equation.

The contents are arranged as:

Firstly, a coefficient which reflects the effects of longitudinal pressure gradient on velocity distribution was introduced in the modified log-wake law (MLWL).

Secondly, this MLWL was validated by compared with high quality experimental data of turbulent nonzero-pressure-gradient flat plate boundary layer flows in wind tunnels (both favorable pressure gradient and adverse pressure gradient). At the same time, corresponding parameters were determined by comparison with the experimental data.

Thirdly, since only a few studies (Termes, 1984; Tsujimoto et al., 1990, Cardoso et al. 1991, and Kironoto et al., 1994) on the effect of non-uniformity (also known as favorable or adverse pressure gradient), carried in for open channels, could be found in the literature, and no corresponding experimental data in open channel flows are available. A series of numerical experiments was carried out by using the famous generic commercial CFD computer program software – FLUENT to validate the MLWL, determine its parameters and illustrate its application in hydraulic engineering.

1.3 LIMITATIONS

All the materials (i.e., air and clear water) involved in this study are limited to incompressible fluid. This limitation results from the fact that the Mach numbers of all relevant phenomena in this study are far small to one (March number = $U / c << 1$), in which U denotes the freestream velocity, c the sound speed. The second limitation is that all the walls in this thesis are smooth, no roughness is considered. Lastly, the MLWL is mainly validated in overlap region and outer region.

1.4 OUTLINE OF THESIS

This thesis contains 7 chapters. The structure is as follows:

a) Chapter 1 briefly introduces the problem under the study, the scope of the present research work and the outline of the thesis.

b) Chapter 2 presents a literature review of exiting research work concerning velocity profiles of flat plate turbulent boundary layer flows and open channel flows

c) Chapter 3 derivates the MLWL for the velocity distribution of turbulent nonzero pressure gradient flat plate boundary layer flow and open-channel flow.

d) Chapter 4 identifies the MLWL with high quality experimental data and determines of corresponding parameters.

e) Chapter 5 performs some patch tests to show that commercial CFD computer program software – FLUENT could be used to simulate the turbulent open-channel flow reliably and accurately.

f) Chapter 6 shows the application of the MLWL in wide open channel flows with a series of numerical experiments and the determination of corresponding parameters. It is also illustrates how the MLWL can be applied in civil engineering.

g) Finally, some major conclusions of the present study are summarized in Chapter 7, and some suggestions for the future research are also proposed.

CHAPTER TWO

LITERATURE REVIEW

2.1 INTRODUCTION

This chapter reviews the previous existing work concerning the velocity distribution for turbulent flat plate boundary layer flows and open-channel flows. It begins by describing the velocity distribution of turbulent boundary layer flows over flat plates in Section 2.2. Then, a review of the velocity profiles of open-channel flows is followed in Section2.3. Section 2.4 summarizes the previous major results and weaknesses.

2.2 VELOCITY PROFILE OF TURBULENT FLAT PLATE BOUNDARY LAYER

In his lecture "On Fluid Motion with Very Small Friction" at the Heidelberg mathematical congress in 1904, Ludwig Prandtl showed how a theoretical treatment could be used on viscous flows in cases of great practical importance. He showed that the flow past a body can be divided into two regions: a very thin layer close to the body (boundary layer) where the viscosity is important, and the remaining region outside this layer where the viscosity can be neglected. With the help of this concept, not only was a physically

convincing explanation of the importance of the viscosity in the drag problem given, but simultaneously, by hugely reducing the mathematical difficulty, a path was set for the theoretical treatment of viscous flows. Boundary layer theory has proved to be exceptionally useful and has given considerable stimulation to research into fluid mechanics since the beginning of 20^{th} century .

Because of the complexities of the governing equations and the complexities of the geometry of the objects involved, the amount of information obtained from the purely theoretical methods is limited. With current and anticipated advancements in the area of computational fluid mechanics, it is likely that computer prediction of forces and complicated flow patterns will become more readily available. Nevertheless, numerical methods in computing flows at high Reynolds numbers only become efficient if the particular layered structure of the flow, as given by the asymptotic theory, is taken into account, as occurs if a suitable grid is used for computation. Boundary layer theory will therefore retain its fundamental place in the calculation of high Reynolds number flows (Schlichting and Gersten, 2000, p.XXII).

Turbulent flows in pipes, zero pressure gradient (ZPG) flat plate boundary layers and open channels are not only three fundamental boundary shear flows but also important in mechanical, aeronautic and hydraulic engineering. These three types of flows have similarities. The flow near the wall can be described by the law of the wall. The flow near the pipe axis, the boundary layer edge and the free surface can be described by the velocity defect law.

The classic logarithmic law (2.1) proposed by Prandtl and von Karman was first developed for pipes and ZPG boundary layers in the early 1930s (White, 1991, p.413):

$$\frac{u}{u_*} = \frac{1}{\kappa}\ln\frac{yu_*}{\nu} + B \tag{2.1}$$

where u denotes time average velocity along the wall, u_* is shear velocity, κ von Karman constant, y distance from the wall, ν fluid kinematic viscosity, B additive constant. Laufer (1954) pointed out that experimental data deviate from the logarithmic law away from the pipe wall. Subsequently Coles (1956) confirmed this behavior for boundary layers and suggested the law of the wake. Coles combined the logarithmic law and the wake law produced the log-wake law,

$$\frac{u}{u_*} = \left(\frac{1}{\kappa}\ln\frac{yu_*}{\nu} + B\right) + W(\xi) \tag{2.2}$$

in wich $\xi = y/\delta$ denotes the relative distance from the wall, and δ is the boundary layer thickenss which is defined by $u(y=\delta) = 0.999U$ in this thesis, U denotes freestream velocity, $W(\xi)$ is the law of the wake which defines the deviation from the logarithmic law away from the wall. Coles (1956) used an empirical table to describe the wake function $W(\xi)$. Hinze (1975, p.698) fit the Coles data analytically, i.e.

$$W(\xi) = \frac{2\Pi}{\kappa}\sin^2\frac{\pi\xi}{2} \tag{2.3}$$

in which Π is called the Coles' wake strength which accounts for the effects of Reynolds number in ZPG boundary layers. Including Hinze's equation (2.3) the log-wake law (LWL) (2.2) is often written as

$$\frac{u}{u_*} = \left(\frac{1}{\kappa} \ln \frac{y u_*}{\nu} + B \right) + \frac{2\Pi}{\kappa} \sin^2 \frac{\pi \xi}{2} \tag{2.4}$$

This log-wake law has been studied and applied extensively. But comparison of equation (2.4) with experimental data (Coles,1969; Hinze, 1975, p.699) showed that (2.4) is invalid near the boundary layer edge where the zero velocity gradient requirement is not satisfied.

Recently, Guo and Julie (2003) proposed a modified log-wake law for pipes, which improves the conventional log-wake law by meeting the zero velocity gradient requirement at the axis. Based on the same concept, Guo et al.(2003) proposed another modified log-wake law (MLWL) (2.5) to improve (2.4) by satisfying the zero velocity gradient requirement at the boundary layer edge.

$$\frac{u}{u_*} = \left(\frac{1}{\kappa} \ln \frac{y u_*}{\nu} + B \right) + \frac{2\Pi}{\kappa} \sin^2 \frac{\pi \xi}{2} - \frac{\xi^3}{3\kappa} \tag{2.5}$$

where the last term is a cubic correction which causes the improvement. Comparison of (2.5) with recent experimental data showed that (2.5) agrees with experiment data fairly perfect and completely satisfy the zero velocity gradient requirement at the edge of boundary layer (Guo et al., 2003).

The conventional log-wake law (2.4) is usually not only employed to describe the ZPG boundary layer flows but also to simulate the NPG boundary layer flows. In the former situation, the wake strength Π is a constant. In the latter situation, Π becomes a variable reflects the effects of pressure gradient for the velocity distribution. Clauser (1956) used a dimensionless parameter $\beta = (\delta^* / \tau_w) dp/dx$ to represent the magnitude of pressure

gradient, where δ^* is the displacement thickness of boundary layer, τ_w the wall shear stress, dp/dx the longitudinal pressure gradient. Based on the traditional log-wake law (2.4), Das (1987) has correlated hundreds of data points from the 1968 Stanford Conference into the following second-order polynomial correlation (White, 1991, p.451):

$$\beta = -0.4 + 0.76\Pi + 0.42\Pi^2 \tag{2.6}$$

The parameter Π can be determined by (2.6) when the Clauser pressure gradient parameter β is measured in a boundary layer. Then, the velocity distribution can be predicted by (2.4).

Because of the emergence of the cubic correction term in the MLWL, the magnitude of Π in the MLWL (2.5) should not be equal to that in the LWL (2.4). The main objective of this thesis is to apply the modified log-wake law to the turbulent NPG flat plate boundary layer flows and determine the new correlation of Π with β based on MLWL.

2.3 VELOCITY PROFILE OF OPEN-CHANNEL FLOW

Knowledge of the mean velocity distribution in open-channel flow is of importance in hydraulic engineering. The uniform open-channel flow has been studied in great detail, but the knowledge about the velocity profile of nonuniform (accelerating and decelerating) open-channel flows is still insufficient and incomplete.

Since Keulegan (1938) suggested the logarithmic velocity distribution (log law) to hold over the entire depth of open-channel flow, this law has been widely used in hydraulic

engineering. However, more precise investigates (Coleman, 1981, 1986, Nezu and Rodi, 1986, Kironoto and Graf, 1994) showed that the log law is only valid in the region near the wall; far from the wall the mean velocity profile deviates from the log law. Like in flat plate boundary layer and closed duct flows, two regions – of mean velocity – were also suggested in open-channel flow: the inner region, where the log law is valid, and the outer region, where the velocity profiles do not follow the log law.

The log-wake law (2.4) has been employed to account for the deviation in the outer region, too. Tonimaga and Nezu (1992) experimentally showed that additive constant B is about 5.29 for subcritical flow while it decreases with Froude number for supercritical flow. About the wake strength Π, obtained in uniform open channel are showed in Table 2.1.

Table 2.1 Experimental value of wake strength Π in uniform open channel

No.	Experimenter	Time	Π	Remark
1	Coleman	1981, 1986	0.19	
2	Nezu and Rodi	1986	0.11 ~ 0.253	Smooth bed
3	Kirkgoz	1989	0.1	
4	Cardoso et al.	1989	-0.077	Smooth bed,
5	Kironoto and Graf	1994	-0.08 ~ 0.16	Rough bed,

One can see that a universal of Π may therefore not exist, but the range of the value of Π can be concluded as $-0.08 < \Pi < 0.25$ in uniform open-channel flow.

Until the present time, however, the knowledge of the mean flow in nonuniform open-channel flow is incomplete. Only a few studies, the one by Termes (1984), Tsujimoto et al. (1994), Cardoso et al. (1991), and Kironoto and Graf (1995), investigated the non-uniformity of the flow. Non-uniform open-channel flow has the same form of governing equation as NPG boundary layers. Hence, the log-wake law was employed to describe the mean velocity distribution of open-channel flow by Kironoto (1992), Kironoto and Graf (1995). They carried out a correlation of Π with $\beta = (\delta^* / \tau_w) dp^* / dx$ and another correlation of Π with a new pressure gradient parameter $\beta_h = (h / \tau_w) dp^* / dx$ for open channels, in which h denotes the water depth, τ_w the wall shear stress, dp^* / dx the longitudinal total pressure gradient:

$$\Pi = 0.75(\beta + 0.5)^{0.75} - 0.22 \tag{2.7}$$

or

$$\Pi = 0.08\beta_h + 0.23 \tag{2.8}$$

It should be noted that Kironoto and Graf asserted that above equations were valid for wide open-channel flow (2D), but those two formulae were constructed based on their experimental data gained in rough narrow open channel.

As reported by Lemmin and Rolland (1997), under the effects of sidewall and the damping influence of the free surface, the velocity dip may also occur in natural wide channel at large width-depth ratios, e.g., w/h = 20 ~ 40. It means the maximum velocity occurs under the free surface is an ordinary reality and the zero velocity gradient requirement also exist in most cases of open-channel flows. Unfortunately, the log-wake

law (2.4) does not satisfy this boundary condition. To overcome this shortcoming, the MLWL seems a good solution. Actually, the MLWL can simulate the velocity profile from the overlap region to the free surface including the velocity dip phenomenon in wide open channel.

2.4 SUMMARY

The traditional log-wake law (LWL) can not meet the zero velocity gradient requirement at the boundary layer edge. Guo et al. (2003) proposed a modified log-wake law (MLWL) for ZPG flat plate boundary layer flows, which improve the conventional log-wake law by meeting the zero velocity gradient requirement at the boundary layer edge. Furthermore, the MLWL can reflect the velocity dip phenomenon which universally exists in open channels. Whether the modified log-wake law is valid or not for nonzero-pressure-gradient (NPG) flat plate boundary layer and nonuniform open-channel flows still need to be identified.

CHAPTER THREE

APPLICATION OF MODIFIED LOG-WAKE LAW FOR NPG FLAT PLATE TURBULENT BOUNDARY LAYERS

3.1 INTRODUCTION

This chapter shows how to theoretically apply modified log-wake-law to turbulent nonzero-pressure-gradient (NPG) flat plate boundary layers and open-channel flows. The hypothesis of the modified log-wake law is first introduced in Section 3.2. Secondly, Section 3.3 describes skin friction in the modified log-wake law. Thirdly, a brief summary of the application of modified log-wake law for NPG boundary layers is given in Section 3.4.

3.2 HYPOTHESIS OF THE MODIFIED LOG-WAKE LAW

This section examines the shear stress distribution in NPG boundary layer and constructs a new term to reflect the effects of pressure gradient in MLWL.

3.2.1 SHEAR STRESS DISTRIBUTION

Consider a steady two-dimensional incompressible viscous flow over a flat plate where *x* direction is along the wall and y normal to the wall. The boundary layer equations are (Schlichting and Gerston, 2000, p.514)

$$\frac{\partial u}{\partial x}+\frac{\partial v}{\partial y}=0 \tag{3.1}$$

$$u\frac{\partial u}{\partial x}+v\frac{\partial u}{\partial y}=-\frac{1}{\rho}\frac{\partial p}{\partial x}+\frac{1}{\rho}\frac{\partial \tau}{\partial y} \tag{3.2}$$

where u denotes the time-averaged velocity in the x direction, v the time-averaged velocity in the y direction, ρ the fluid density, p stands for boundary-layer free stream pressure, $\partial p/\partial x$ represents the pressure gradient in the x direction, $\tau=\tau_v+\tau_t=\mu(\partial u/\partial y)-\rho\overline{u'v'}$ the local shear stress that includes viscous shear stress ($\tau_v=\mu(\partial u/\partial y)$) and turbulent shear stress ($-\rho\overline{u'v'}$). Equation (3.1) is the continuity equation, and (3.2) is the momentum equation along the wall.

On the other hand, together with the continuity equation, the system of equations for two-dimensional steady flow such as wide open-channel flow (see Graf and Altinakar, 1993, chap. 2.5) is given by

$$\frac{\partial u}{\partial x}+\frac{\partial v}{\partial y}=0 \tag{3.3}$$

$$u\frac{\partial u}{\partial x}+v\frac{\partial u}{\partial y}=-\frac{1}{\rho}\frac{\partial p^{*}}{\partial x}+\frac{1}{\rho}\frac{\partial \tau}{\partial y} \tag{3.4}$$

$$0=\frac{1}{\rho}\frac{\partial p^{*}}{\partial y}-\frac{\partial \overline{v'^{2}}}{\partial y} \tag{3.5}$$

where u and v are the time-averaged velocity in the longitudinal (x) and the normal (y) directions, respectively. v' denotes the velocity fluctuations in the y direction.

The longitudinal pressure gradient, defining the water-surface slope, is given as

$$\frac{\partial p^{*}}{\partial x}=\rho g\left(-S+\frac{dh}{dx}\right) \tag{3.6}$$

where the bottom slope S is assumed to be small, S << 1, and dh/dx is the longitudinal variation of the water depth h. which represents the variation of the pressure distribution along the x direction in open-channel flow. The local shear stress is the same as in (3.2) $\tau=\tau_{v}+\tau_{t}=\mu(\partial u/\partial y)-\rho\overline{u'v'}$.

Equation (3.5) shows that the vertical pressure distribution is not exactly hydrostatic; however, it is often assumed that hydrostatic pressure prevails (Kironoto and Graf, 1995).

Comparing equations (3.1) and (3.2) with equations (3.3) and (3.4), one can see the governing equations of steady wide open-channel flow (2D) are the same as those of 2D boundary layers if the boundary-layer free stream pressure (p) replaced by the total pressure head (p^{*}). Hence, the following derivation according to equations (3.1) and (3.2) is not only valid in turbulent flat plate boundary layers, but also valid for steady, two-dimensional wide open-channel flows.

Substituting continuity equation (3.1) in to momentum equation (3.2)

$$-u\frac{\partial v}{\partial y}+v\frac{\partial u}{\partial y}=-\frac{1}{\rho}\frac{\partial p}{\partial x}+\frac{1}{\rho}\frac{\partial \tau}{\partial y}$$

Integrate above equation across the boundary layer to develop

$$\frac{1}{\rho}\frac{\partial \tau}{\partial y}=-u\frac{\partial v}{\partial y}+v\frac{\partial u}{\partial y}+\frac{1}{\rho}\frac{\partial p}{\partial x}$$

$$\frac{\partial \tau}{\partial y}=\rho\left(-u\frac{\partial v}{\partial y}+v\frac{\partial u}{\partial y}+\frac{1}{\rho}\frac{\partial p}{\partial x}\right)$$

$$\int_0^y d\tau=\rho\int_0^y\left(-u\frac{\partial v}{\partial y}+v\frac{\partial u}{\partial y}+\frac{1}{\rho}\frac{\partial p}{\partial x}\right)dy$$

$$\tau-\tau_w=\rho\int_0^y\left(-u\frac{\partial v}{\partial y}+v\frac{\partial u}{\partial y}+\frac{1}{\rho}\frac{\partial p}{\partial x}\right)dy$$

$$\tau=\tau_w+\rho\int_0^y\left(-u\frac{\partial v}{\partial y}+v\frac{\partial u}{\partial y}\right)dy+\frac{\partial p}{\partial x}\mathrm{y} \tag{3.7}$$

Where $\tau=\tau_w$ at the wall y = 0. Equation (3.7) is the expression for the shear stress distribution. One can realize that the shear stress in NPG boundary layers includes the contributions of the wall shear stress, convective inertia and pressure gradient.

3.2.2 DIMENSIONAL ANALYSIS OF VELOCITY DISTRIBUTION

In the outer region, the viscous shear stress can be neglected. Applying the eddy viscosity model,

$$\tau_t=\rho\nu_t\frac{du}{dy} \tag{3.8}$$

in which τ_t is the turbulent shear stress and ν_t denotes the eddy viscosity, to (3.7) gives

$$\rho\nu_t \frac{du}{dy} = \tau_w + \rho\int_0^y \left(-u\frac{\partial v}{\partial y} + v\frac{\partial u}{\partial y}\right)dy + \frac{\partial p}{\partial x}y \tag{3.9}$$

Considering that the eddy viscosity can be expressed by (Hinze, 1975)

$$\nu_t = \delta u_* f\left(\frac{y}{\delta}\right) \tag{3.10}$$

in which f is an unknown function, and applying the definitions $\xi = y/\delta$ and $\tau_w = \rho u_*^2$ to (3.9), one obtains

$$\rho\delta u_* f\left(\frac{y}{\delta}\right)\frac{du}{dy} = \rho u_*^2 + \rho\int_0^y \left(-u\frac{\partial v}{\partial y} + v\frac{\partial u}{\partial y}\right)dy + \frac{\partial p}{\partial x}y$$

Both sides divided by ρu_*^2

$$\frac{\delta}{u_*} f\left(\frac{y}{\delta}\right)\frac{du}{dy} = 1 + \int_0^y \frac{1}{u_*^2}\left(-u\frac{\partial v}{\partial y} + v\frac{\partial u}{\partial y}\right)dy + \frac{1}{\rho u_*^2}\frac{\partial p}{\partial x}y$$

rewrite above equation as following

$$f\left(\frac{y}{\delta}\right)\frac{\partial}{\partial \frac{y}{\delta}}\left(\frac{u}{u_*}\right) = 1 + \int_0^y \left[-\frac{u}{u_*}\frac{\partial}{\partial \frac{y}{\delta}}\left(\frac{v}{u_*}\right) + \frac{v}{u_*}\frac{\partial}{\partial \frac{y}{\delta}}\left(\frac{u}{u_*}\right)\right]\frac{dy}{\delta} + \frac{\delta}{\rho u_*^2}\frac{\partial p}{\partial x}\frac{y}{\delta}$$

$$f(\xi)\frac{\partial}{\partial \xi}\left(\frac{u}{u_*}\right) = 1 + \int_0^\xi \left[-\frac{u}{u_*}\frac{\partial}{\partial \xi}\left(\frac{v}{u_*}\right) + \frac{v}{u_*}\frac{\partial}{\partial \xi}\left(\frac{u}{u_*}\right)\right]d\xi + \frac{\delta}{\rho u_*^2}\frac{\partial p}{\partial x}\xi \tag{3.11}$$

Except for the complicated integrodifferential form in the above, the eddy viscosity function $f(\xi)$ is not really specified. Thus, it is impossible to get an analytical solution for u. However, the preceding equation suggests the following dimensionless solution form:

$$\frac{u}{u_*}=F_1\left(\xi,\frac{v}{u_*},\frac{\delta}{\rho \mathrm{u}_*^{\,2}}\frac{\partial p}{\partial x}\right)=F_1\left(\xi,\frac{v}{u_*},\frac{\delta}{\tau_{\mathrm{w}}}\frac{\partial p}{\partial x}\right)$$

in which the dimensionless term $(\delta/\tau_w)dp/dx$ represents the pressure gradient in the x direction. The nonzero-pressure-gradient boundary layers can be regarded as zero-pressure-gradient boundary layers superposed effects of pressure gradients. It's reasonable to decompose the right side of above equation into two components:

$$\frac{u}{u_*}=F\left(\xi,\frac{v}{u_*}\right)+P\left(\xi,\frac{\delta}{\rho u_*^{\,2}}\frac{\partial p}{\partial x}\right) \tag{3.12}$$

in which

$$\frac{v}{u_*}=\eta(\xi) \tag{3.13}$$

η is the velocity distribution function in the y direction, and F and P are the velocity distribution functions in the x direction. Substituting (3.13) into (3.12) gives

$$\frac{u}{u_*}=F(\xi,\eta)+P\left(\xi,\frac{\delta}{\rho u_*^{\,2}}\frac{\partial p}{\partial x}\right) \tag{3.14}$$

The effect of pressure gradient on the velocity distribution is reflected in the function $P(\xi,\partial p/\partial x)$. On the other hand, the function $F(\xi,\eta)$ does not involve the effect of pressure gradient, i.e., the function $F(\xi,\eta)$ represents the velocity distribution for turbulent zero-pressure-gradient boundary layers. The function $F(\xi,\eta)$ and its corresponding parameters were decided by Guo et al. (2003). In order to explain the modified log-wake law clearly, some details of the derivation of $F(\xi,\eta)$ will be given in the following analysis. The function $P\left(\xi,\left(\delta/\rho u_*^{\,2}\right)\partial p/\partial x\right)$ will be discussed in § 3.2.3.4.

Since the transverse velocity *v* or η is very small compared with the primary velocity *u* or *F* in the outer region, one can approximate the $F(\xi,\eta)$ by expansion at η = 0, i.e.

$$F(\xi,\eta) = F(\xi,0) + \eta\frac{\partial F(\xi,0)}{\partial \eta} + \frac{\eta^2}{2!}\frac{\partial^2 F(\xi,0)}{\partial \eta} + \cdots \tag{3.15}$$

Taking the first two terms approximation, one has

$$F(\xi,\eta) = F(\xi,0) + \eta\frac{\partial F(\xi,0)}{\partial \eta} \tag{3.16}$$

Note that the above analysis is equivalent to a small perturbation introduced by the transverse velocity function $\eta(\xi)$.

3.2.3 APPROXIMATION OF THE VELOCITY DISTRIBUTION

3.2.3.1 THE PRIMARY FUNCTION $F(\xi,0)$

The functions $F(\xi,0)$, $\eta(\xi)$ and $\partial F(\xi,0)/\partial\eta$ are approximated asymptotically and empirically. First, consider the overlap region where the effect of the transverse velocity *v* or η can be neglected and $\partial F(\xi,0)/\partial\eta$ is finite. One can conclude that the primary function $F(\xi,0)$ is the law of the wall which is often described by the classical logarithmic law or the power law. Recently based on many experimental velocity profiles, Barenblatt et al. (2000) showed that a Reynolds number dependent power law can also represent the velocity profile in the overlap region. Thus an assumption that the following law of the wall is reasonable:

$$\frac{u}{u_*} = \left(a \ln \mathrm{Re}_\delta + b\right)\left(\frac{yu_*}{\nu}\right)^{c/\ln \mathrm{Re}_\delta} \tag{3.17}$$

in which a, b and c are positive constants and the Reynolds number Re_δ is defined as

$$\mathrm{Re}_\delta = \frac{\delta u_*}{\nu} \tag{3.18}$$

which is only slightly different from the original version in Barenblatt et al. (2000). Since the power exponent $c/\ln \mathrm{Re}_\delta$ in equation (3.17) is usually very small say 0.1~0.15 (Barenblatt et al., 2000), one can rewrite (3.17) by series expansion as

$$\begin{aligned}
\frac{u}{u_*} &= \left(a \ln \mathrm{Re}_\delta + b\right)\left(\frac{yu_*}{\nu}\right)^{c/\ln \mathrm{Re}_\delta} \\
&= \left(a \ln \mathrm{Re}_\delta + b\right)\exp\left\{\frac{c}{\ln \mathrm{Re}_\delta}\ln\left(\frac{yu_*}{\nu}\right)\right\} \\
&= \left(a \ln \mathrm{Re}_\delta + b\right)\left\{1 + \frac{c}{\ln \mathrm{Re}_\delta}\ln\left(\frac{yu_*}{\nu}\right) + \frac{1}{2!}\left[\frac{c}{\ln \mathrm{Re}_\delta}\ln\left(\frac{yu_*}{\nu}\right)\right]^2 + \cdots\right\} \\
&= \left(a \ln \mathrm{Re}_\delta + b\right) + \left(ac + \frac{bc}{\ln \mathrm{Re}_\delta}\right)\ln\left(\frac{yu_*}{\nu}\right) + \cdots
\end{aligned}$$

In the overlap region, one has $y << \delta$ or $\ln(yu_*/\nu) << \ln \mathrm{Re}_\delta$, the above equation can then be approximated as

$$\frac{u}{u_*} = \left(a \ln \mathrm{Re}_\delta + b\right) + \left(ac + \frac{bc}{\ln \mathrm{Re}_\delta}\right)\ln\left(\frac{yu_*}{\nu}\right) \tag{3.19}$$

Comparing it with the classical logarithmic law, one has

$$\frac{1}{\kappa} = ac + \frac{bc}{\ln \mathrm{Re}_\delta} \to ac \tag{3.20}$$

for large Reynolds number, and

$$B = a \ln \mathrm{Re}_\delta + b \tag{3.21}$$

where B = additive constant. Note that equation (3.20) and (3.21) show that:

a) The von Karman constant κ increases with Reynolds number;

b) A universal von Karman constant κ may exist only for large Reynolds number;

c) The additive constant B increases with Reynolds number even for large Reynolds number.

The dependence of Reynolds number accounts for the effect of the "viscous superlayer" (Hinze, 1975, p.567) which is near the boundary layer edge where Kolmogoroff length scale energy dissipation exists. In fact, Hinze (1975, p.628) has noticed that the von Karman constant κ varies slightly about 0.4 whereas the additive constant B corresponds with much greater variations, which may be explained by (3.20) and (3.21). For simplicity, Guo's equation concentrates on large Reynolds number and assumes

$$\kappa = \frac{1}{ac} = 0.4 \tag{3.22}$$

Furthermore, the primary function $F(\xi,0)$ can be approximated by (3.19), i.e.

$$F(\xi,0) = \frac{1}{\kappa}\ln\frac{yu_*}{\nu} + B \tag{3.23}$$

in which κ = 0.4 and B is estimated by (3.21) where the constants a and b will be specified in Section 3.3.

3.2.3.2 THE TRANSEVERSE VELOCITY DISTRIBUTION FUNCTION $\eta(\xi)$

It is assumed that the shape of the function $\eta(\xi)$ is similar to its counterpart in laminar flows. Inspired by the Blasius solution and the conventional sine-square wake function, one may assume

$$v = V \sin^2 \frac{\pi\xi}{2} \tag{3.24}$$

in which V is the transverse velocity at the boundary layer edge. Comparing (3.24) with (3.13), one must have

$$V = \chi u_* \tag{3.25}$$

where χ is a proportional constant. With (3.25), equation (3.24), can be rewritten as

$$\frac{v}{u_*} = \eta(\xi) = \chi \sin^2 \frac{\pi\xi}{2} \tag{3.26}$$

The constant χ will be considered together with the derivative function $\partial F(\xi,0)/\partial\eta$.

3.2.3.3 THE DERIVATIVE FUNCTION $\partial F(\xi,0)/\partial\eta$

With (3.26) one can write the second term in (3.16) as

$$\eta \frac{\partial F(\xi,0)}{\partial \eta} = \chi \frac{\partial F(\xi,0)}{\partial \eta} \sin^2 \frac{\pi\xi}{2} \tag{3.27}$$

which is the same as Hinze's version of the law of wake assuming

$$\chi \frac{\partial F(\xi,0)}{\partial \eta} = \frac{2\Pi_0}{\kappa} \tag{3.28}$$

and $\partial F(\xi,0)/\partial\eta$ is independent of ξ. In other words, the second term in (3.16) can be approximated by the conventional law of the wake, i.e.

$$\eta \frac{\partial F(\xi,0)}{\partial \eta} = \frac{2\Pi_0}{\kappa} \sin^2 \frac{\pi\xi}{2} \tag{3.29}$$

According to Coles (Fernholz and Finley, 1996), the wake strength Π increases with Reynolds number and tends to a constant for large Reynolds number. To be consistent with (3.22) where an assumption of large Reynolds number is employed, one can assume

$$\Pi_0 = \text{constant} \tag{3.30}$$

Substituting (3.23) and (3.29) into (3.16) produces the conventional log-wake law (2.4) except that the additive constant *B* varies with Reynolds number.

3.2.3.4 THE PRESSURE GRADIENT FUNCTION $P\left(\xi, \frac{\delta}{\rho u_*^2}\frac{\partial p}{\partial x}\right)$

After the investigation of many velocity profiles, Coles (1968) has clearly shown, mainly for zero and adverse pressure-gradient boundary layers, that deviations from the log law in the outer region can be accounted for by means of the wake function. The pressure gradient function can be directly expressed as

$$P\left(\xi, \frac{\delta}{\rho u_*^2}\frac{\partial p}{\partial x}\right) = \frac{2\Pi_p}{\kappa} sin^2\frac{\pi\xi}{2} \tag{3.31}$$

In above equation, Π_p is a variable relevant to the longitudinal pressure gradient. Usually, a dimensionless parameter, Chauser pressure gradient parameter $\beta = (\delta^*/\tau_w)dp/dx$, is employed to represent the longitudinal pressure gradient. So Π_p is in terms of Clauser pressure gradient parameter β, i.e.

$$\Pi_p = f_1(\beta) \tag{3.32}$$

in which f_1 is a unknown function. The correlation of $\Pi = \Pi_0 + \Pi_p$ with β will be decided together by comparison with experimental data in Section 4.1.

3.2.3.5 BOUNDARY CORRECTION

Strictly speaking, boundary layer do not have edges; the mean velocity is only asymptotic to the free stream velocity at the so-called boundary layer edges, i.e., $u \to U$ at $\xi = y/\delta = 1$. However, in practice the assumptions of

$$u(\xi = 1) = U \tag{3.33}$$

and

$$\left.\frac{du}{d\xi}\right|_{\xi=1} = 0 \tag{3.34}$$

are good approximations. To meet the zero velocity gradient requirement (3.34), one must modify (2.4) by adding a boundary correction function. Guo at el. (2003) have shown that a cubic correction is a good approximation for ZPG boundary layer edge in equation (2.5). The same correction function should be retained for NPG boundary layer, i.e.

$$-\frac{\xi^3}{3\kappa} \tag{3.35}$$

3.2.3.6 THE MODIFIED LOG-WAKE LAW AND ITS DEFECT FORM

Combining (2.4), (3.31) and (3.35) leads to the following velocity profile model:

$$\begin{aligned}\frac{u}{u_*} &= \left(\frac{1}{\kappa}\ln\frac{yu_*}{\nu} + B + \frac{2\Pi_0}{\kappa}\sin^2\frac{\pi\xi}{2} - \frac{\xi^3}{3\kappa}\right) + \frac{2\Pi_p}{\kappa}\sin^2\frac{\pi\xi}{2} \\ &= \frac{1}{\kappa}\ln\frac{yu_*}{\nu} + B + \frac{2}{\kappa}\left(\Pi_0 + \Pi_p\right)\sin^2\frac{\pi\xi}{2} - \frac{\xi^3}{3\kappa} \\ &= \frac{1}{\kappa}\ln\frac{yu_*}{\nu} + B + \frac{2\Pi}{\kappa}\sin^2\frac{\pi\xi}{2} - \frac{\xi^3}{3\kappa}\end{aligned} \tag{3.36}$$

Equation (3.36) differs from the prototype of modified log-wake law (MLWL) for the turbulent NPG flat plate boundary layer flows because of the addition of term $\frac{2\Pi_p}{\kappa}\sin^2\frac{\pi\xi}{2}$. The terms in the parentheses are the MLWL for ZPG flat plate boundary layer flows (Guo, et al., 2003).

The main difference between (3.36) and (2.5) is that: in (3.36), the wake strength Π_p is a variable which changes with pressure gradient for different NPG boundary layers while Π_0 is a constant for all ZPG boundary layers in (2.5). Actually, the modified log-wake law (2.5) for turbulent ZPG flat plate boundary layer flows, in which the wake strength Π_0 is a constant, is a special case of equation (3.36) when $\Pi_p = 0$, $\beta = 0$ result in $\Pi = \Pi_0$.

Similar to turbulent ZPG flat plate boundary layer flows (Guo et al., 2003), the equation (3.36) is the application of the modified log-wake law (MLWL) which should be valid from the overlap region till the boundary layer edge. Equation (3.36) is different from the conventional log-wake law in two aspects: it meets the zero velocity gradient at the boundary layer edge; and the additive constant *B* accounts for the effect of the Reynolds

number. In equation (3.36), the Coles' wake strength $\Pi = \Pi_0 + \Pi_p$, varied with the pressure gradient.

To eliminate the effect of Reynolds number in (3.36), one can introduce the freestream velocity U at $\xi = 1$ to the modified log-wake law. From (3.36), one obtains

$$\frac{U}{u_*} = \left(\frac{1}{\kappa} \ln \frac{\delta u_*}{\nu} + B \right) + \frac{2\Pi}{\kappa} - \frac{1}{3\kappa} \tag{3.37}$$

Subtracting (3.36) from (3.37) gives the velocity defect form of the modified log-wake law

$$\begin{aligned} \frac{U-u}{u_*} &= \frac{1}{\kappa}\left(\ln \xi - 2\left(\Pi_0 + \Pi_p\right)\cos^2 \frac{\pi\xi}{2} + \frac{1-\xi^3}{3} \right) \\ &= \frac{1}{\kappa}\left(\ln \xi - 2\Pi \cos^2 \frac{\pi\xi}{2} + \frac{1-\xi^3}{3} \right) \end{aligned} \tag{3.38}$$

After tested the MLWL with experimental data of turbulent ZPG flat plate boundary layers, Guo et al. (2003) found that the velocity defect form in the outer region including the overlap region is independent of Reynolds number. It implies that the model parameters κ and Π_0 in the modified log-wake law (3.38) are universal constants. They suggested the universal value of κ and Π_0:

$$\kappa = 0.4 \tag{3.39}$$

and

$$\Pi_0 = 0.7577 \tag{3.40}$$

However, Π_p is a variable that changes with β. $\Pi = \Pi_0 + \Pi_p$ therefore is a variable changes with β. The correlation of Π with β will be defined in Chapter 4.

3.3 SKIN FRICTION AND THE ADDITIVE CONSTANT IN THE MODIFIED LOG-WAKE LAW

One can compute the velocity profile by using the velocity defect law (3.38) which does not require the additive constant *B*. Nevertheless, if the modified log-wake law (3.36) is preferred, the additive constant *B* can be defined by studying the skin friction factor c_f which is defined as

$$\tau_w = \frac{c_f}{2}\rho U^2 \tag{3.41}$$

According to the definition $u_* = \sqrt{\tau_* / \rho}$, (3.41) can be rewrite as

$$\sqrt{\frac{2}{c_f}} = \frac{U}{u_*} \tag{3.42}$$

Substituting (3.21) into (3.37) gives

$$\frac{U}{u_*} = \left(\frac{1}{\kappa} + a\right)\ln \mathrm{Re}_\delta + \left(b + \frac{2\Pi}{\kappa} - \frac{1}{3\kappa}\right) \tag{3.43}$$

which can be rearranged as

$$\sqrt{\frac{2}{c_f}} = \frac{U}{u_*} = \frac{1}{\kappa_1}\ln \mathrm{Re}_\delta + B_1 \tag{3.44}$$

where

$$\frac{1}{\kappa_1} = \frac{1}{\kappa} + a \tag{3.45}$$

$$B_1 = b + \frac{2\Pi}{\kappa} - \frac{1}{3\kappa} \tag{3.46}$$

are determined experimentally. After compared with experimental data, Guo et al. suggested

$$a = 0.1176 \tag{3.47}$$

$$b = 3.6544 \tag{3.48}$$

$$\kappa_1 = 0.3820 \tag{3.49}$$

$$B_1 = 6.6040 \tag{3.50}$$

For turbulent NPG flat plate boundary layers, B_1 is a function in terms of Π, i.e

$$B_1 = 3.6544 + \frac{2\Pi}{0.4} - \frac{1}{3\times 0.4} = 2.8211 + 5\Pi \tag{3.51}$$

While Π is determined, the velocity distribution and the wall shear stress could be evaluated by equation (3.38) and (3.44), respectively.

The skin friction factor c_f is often correlated with the momentum thickness Reynolds number Re_θ, i.e.

$$\mathrm{Re}_\theta = \frac{\theta U}{\nu} \tag{3.52}$$

$$c_f = f\left(\mathrm{Re}_\theta\right) \tag{3.53}$$

in which θ means the momentum thickness. For a specific velocity profile, the value of Coles' wake strength Π is a specific constant. The displacement thickness δ^* and the momentum thickness θ can be estimated from the Modified log-wake law (3.35) which gives

$$\int_0^1 \frac{u}{u_*} d\xi = -\frac{1}{\kappa}\left(\Pi + \frac{3}{4}\right) + \frac{U}{u_*} \tag{3.54}$$

and

$$\begin{aligned}\int_0^1 \left(\frac{u}{u_*}\right) d\xi = &-\frac{1}{\kappa^2}\left(\frac{81}{56} + \frac{3\Pi}{2} - \frac{2\Pi}{\pi^2} + \frac{8\Pi}{\pi^4} + \frac{2\Pi Si(\tau)}{\pi} + \frac{3\Pi^2}{\pi}\right) \\ &-\frac{2}{\kappa}\left(\frac{3}{4} + \Pi\right)\frac{U}{u_*} + \left(\frac{U}{u_*}\right)^2\end{aligned} \tag{3.55}$$

Applying (3.51) to the definition of the displacement thickness δ_*,

$$\frac{\delta_*}{\delta} = \int_0^1 \left(1 - \frac{u}{u_*}\right) d\xi = 1 - \frac{u_*}{U}\int_0^1 \frac{u}{u_*} d\xi = \frac{1}{\kappa}\left(\Pi + \frac{3}{4}\right)\frac{u_*}{U} \tag{3.56}$$

Applying (3.45) and (3.46) to the definition of the momentum thickness θ gives

$$\frac{\theta}{\delta} = \int_0^1 \frac{u}{U}\left(1 - \frac{u}{U}\right) d\xi = \frac{u_*}{U}\int_0^1 \frac{u}{u_*} d\xi - \left(\frac{u_*}{U}\right)^2 \int_0^1 \left(\frac{u}{u_*}\right) d\xi = \alpha\left(\frac{u_*}{U}\right)^2 + \zeta\left(\frac{u_*}{U}\right) \tag{3.57}$$

in which

$$\begin{aligned}\alpha &= -\frac{81}{56\kappa^2} - \left(\frac{3}{4} + \frac{Si(\pi)}{\pi} - \frac{1}{\pi^2} + \frac{4}{\pi^4}\right)\frac{2\Pi}{\kappa^2} - \frac{3\Pi^2}{2\kappa^2} \\ &= -\frac{1.4464 + 2.5585\Pi + 1.5\Pi^2}{\kappa^2}\end{aligned} \tag{3.58}$$

$$\zeta = \frac{1}{\kappa}\left(\frac{3}{4} + \Pi\right) \tag{3.59}$$

Furthermore,

$$\mathrm{Re}_\delta = \frac{\delta u_*}{\nu} = \frac{\theta U}{\nu}\frac{\delta}{\theta}\frac{u_*}{U} = \mathrm{Re}_\theta\left(\alpha\sqrt{\frac{c_f}{2}} + \zeta\right)^{-1} \tag{3.60}$$

For ZPG flows, Coles' wake strength is an universal constant $\Pi = \Pi_0 = 0.7577$, one can gets

$$\alpha = -26.538 \tag{3.61}$$

$$\zeta = 3.7693 \tag{3.62}$$

Combining (3.60) and (3.44), the relationship between c_f and Re_θ can be described as

$$\sqrt{\frac{2}{c_f}} = \frac{1}{\kappa_1}\ln \mathrm{Re}_\theta - \frac{1}{\kappa_1}\ln\left(\alpha\sqrt{\frac{c_f}{2}} + \zeta\right) + B_1 \tag{3.63}$$

in which the constants in (3.49) and (3.51) are used for the values of κ_1 and B_1. Combining (3.44) and (3.63) provides a method to estimate the wall shear stress τ_w and the boundary layer thickness δ from a measured velocity profile. The details of procedure will be introduced and applied in Section 4.3.

3.4 SUMMARY

The modified log-wake law (MLWL) consists of three terms:

a) A logarithmic term in which the von Karman constant is about 0.4 while the additive constant increases with Reynolds number; reflects the effect of the wall shear stress and is dominant in the overlap region;

b) A sine-square term with a wake strength; approximates the transverse velocity, reflects the effect of convective inertia and pressure gradient.

c) A cubic correction term, makes the conventional log-wake law satisfy the zero velocity gradient requirement at the boundary layer edge.

CHAPTER FOUR

VALIDATION OF MODIFIED LOG-WAKE LAW FOR NPG FLAT PLATE TURBULENT BOUNDARY LAYERS

4.1 INTRODUCTION

As shown in previous chapters, the modified log-wake law (MLWL) (3.36) or its defect form (3.38) was developed from (2.5) which was proposed to simulate the turbulent zero-pressure-gradient flat plate boundary layers. Is it suitable to simulate the turbulent nonzero-pressure-gradient flat plate boundary layer flows? In this chapter, validations will be done by comparing the MLWL with high quality experimental data of turbulent nonzero-pressure-gradient flat plate boundary layers.

Section 4.2 describes the general methodology of validation. Then, the modified log-wake law is compared with eight different experiment datum sets in eight sections (Section 4.3

to Section 4.10). Section 4.11 depicts the relationship between Clauser pressure gradient parameter β and Coles' wake strength Π. Section 4.12 is a brief summary of this chapter.

4.2 METHODOLOGY

For convenience, one can rewrite the velocity defect form (3.35) of the modified log-wake law as

$$\frac{u}{u_*}=\frac{U}{u_*}-\frac{1}{\kappa}\left(\ln\xi-2\Pi\cos^2\frac{\pi\xi}{2}+\frac{1-\xi^3}{3}\right) \tag{4.1}$$

When the modified log-wake law (3.36) or its defect form (4.1) is employed to simulate the velocity profiles of ZPG flat plate turbulent boundary layers, all coefficients involved in this equation (i.e., κ and $\Pi=\Pi_0$) are universal constants. Conversely, for turbulent NPG flat plate boundary layers, the Coles wake strength $\Pi=\Pi_0+\Pi_p$ is no longer a constant. The variation of the Coles wake strength Π reflects the effects of pressure gradient on velocity distribution. According to previous study, in NPG flat plate boundary layer, Π is a function in terms of pressure gradient which is always depicted by the Clauser pressure gradient parameter $\beta=\left(\delta^*/\tau_w\right)dp/dx$. Based on the conventional log-wake law, the relationship of Π and β was described by equation (2.6) which was summarized by Das (1987) according to hundreds of experimental data points.

Hence, the identifying procedure consists of three main parts:

a) Check structure of the MLWL

Comparison of the MLWL with the experimental data of velocity profiles for turbulent NPG boundary layer flows is the most convictive and intuitionistic method. If the structure of MLWL is not correct, it can not simulate the experimental velocity profiles well. If the MLWL agree with the experimental data well, one can say its structure is correct.

In this process, only the Coles' wake strength Π is variable, another parameter involved in the defect form (4.1) is κ which keeps as an universal constant. A parametric curve fit of the MLWL (3.36) or its defect form (4.1) to the experimental data could determine the specific value of Π for each specific boundary layer.

b) Determine the correlation of Π with β

There are a specific value of β and a specific value of Π for each boundary layer velocity profile. In the first step, a series of Π corresponding to a series of β are gotten. The correlation of Π with β could be decided by curve fit with a second-order polynomial. One can use this correlation to determine the value of Π for a measured velocity profile in a pressure gradient domain.

Because the effects of cubic correction term in (4.1) are focus on the boundary layer edge, the values of Π gotten in (4.1) should not far different from the values of Π gotten from

(2.6). Some similarities therefore should exist between the new relationship and Das' formula (2.6).

c) The skin friction factor c_f

The skin friction factor c_f represents the corresponding wall shear stress τ_w, is a very important coefficient for boundary layer theory. The comparison of the c_f values predicted by equation (3.63) with the real experimental data also will be given.

The modified log-wake law (3.36) and its velocity defect form (4.1) have the same physical significance. On the other hand, the velocity defect form (4.1) of the modified log-wake law eliminates the effect of Reynolds number represented by the constant B in equation (3.36). In most of the relevant experiments, the free stream velocity U at the boundary layer edge $y=\delta(\xi=1)$ is given. For simplification, in the following analysis, the velocity defect form (4.1) is preferred to be employed.

In order to illustrate the MLWL well, a traditional logarithmic law is also compared in the velocity profile figure in this chapter. The log law used in this chapter and its coefficient is

$$\frac{u}{u_*}=\frac{1}{\kappa}\ln\frac{yu_*}{\nu}+B=\frac{1}{0.4}\ln\frac{yu_*}{\nu}+0.1176\ln\mathrm{Re}_\delta+3.6544 \tag{4.2}$$

The boundary layer thickness δ is defined by $u(y=\delta)=0.999U$ in this thesis.

4.3 TEST WITH M. B. JONES' EXPERIMENTAL DATA (FPG)

4.3.1 BASIC INFORMATION OF JONES' EXPERIMENTS

There are 63 favorable pressure gradient (FPG) experimental velocity profiles by M. B. Jones can be found on his homepage http://www.mame.mu.oz.au/~mbjones/sinkflow.html. These data are the experimental results of Jones' Ph.D Thesis (1998).

Jones' experiments were performed in an open-return blower wind tunnel. Details of the working section are shown in figure 4.1. The smooth acrylic floor of the working section provides the "smooth wall" on which the boundary layer develops. The trip wire was placed at $x = 0$ arbitriarily. The pressure gradient for all experiments was controlled by a straight rigid ceiling hinged at the begining of the work section.

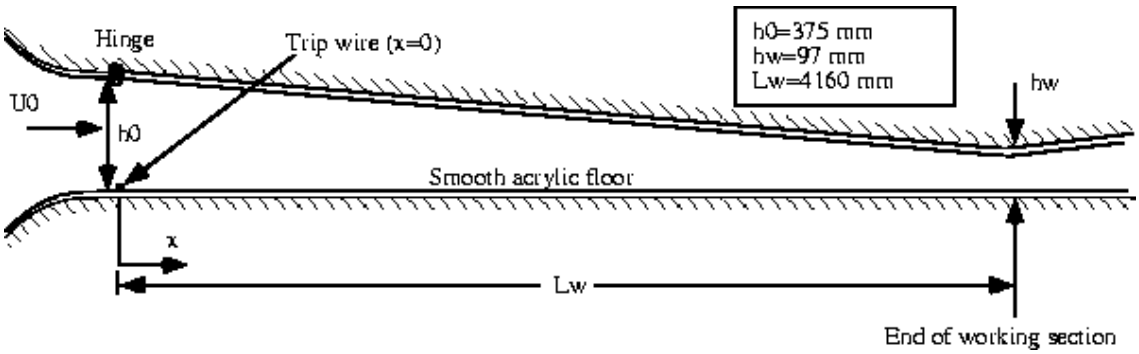

FIG. 4.1 Working section geometry of Jones' experiments

4.3.2 VELOCITY PROFILES

A sink flow can be uniquely characteized by the acceleration parameter K which is difined as

$$K = \frac{\nu}{U^2}\frac{dU}{dx} \tag{4.3}$$

where ν is the kinematic viscosity of the fluid, U the local free-stream velocity, x the steamwise coordinate.

The results presented in the webside are from experiments in sink flows at three levels of acceleration: $K = 2.70\times10^{-7}$, 3.59×10^{-7} and 5.39×10^{-7}. For each flow case, mean proflies at 20 ~ 23 streamwise stations were measured, from station x = 180 to 3620 mm. Each mean velocity profile is shown in Figures 4.2 to 4.4. One can see the logarithmic law collapses in the outer region near the boundary layer edge. In contrast, the profiles are well described by the modified log-wake law given in (4.1).

Figures 4.2 to 4.4 compare (4.1), in which the constants suggested by Guo et al. (2003) except the wake strength Π are used, with all 63 experimental profiles individually and display excellent agreement for almost all profiles. The parameter Π gotten in the curve fit process for each velocity profile is shown in Tables 4.1 to 4.3. The correclation of Π with β will be treated with other experimental data in Section 4.11.

These figures lead to the following conclusions:

a) The basic structure of the MLWL is correct;

b) The MLWL is suitabel to simulate the turbulent NPG flat plate boundary layers;

c) The MLWL can replicate the experimental data from the overlap ragion till the boundary layer edge, i.e., $30 \le yu_* / \nu$ and $\xi = y/\delta = \left(yu_* / \nu\right)/\mathrm{Re}_\delta \le 1$;

d) The MLWL tends to a straight line in a semilog plot in the overlap region and then concides with the logarithmic law;

e) The zero velocity gradient at the boundary layer edge can be clearly seen from all profiles in Figs. 4.2 to 4.4 which imply that the boundary correction is necessary.

4.3.3 SKIN FRICTION FACTOR c_f

As introdueced in Section 3.3, combining equations (3.49), (3.51), (3.58), (3.59) and (3.63) provides a method to estimate the skin friction factor c_f from a measured velocity profile of a turbulent NPG flat plate boundary layer flow. One can predict the value of c_f by following the procedure step by step:

a) Calculate the momentum thickness θ by applying a measured velocity profile to the definition of the momentum thickness;

b) Estimate the value of Π by equation (4.4). For convenience, the value of Π gained in the curve fit is used directly in this validation.

c) Computer the value of coefficients B_1, α and ζ.

d) Estimate the friction factor c_f from (3.63);

When c_f is gotten, the wall shear stress τ_w or the shear velocity u_* and boundary layer

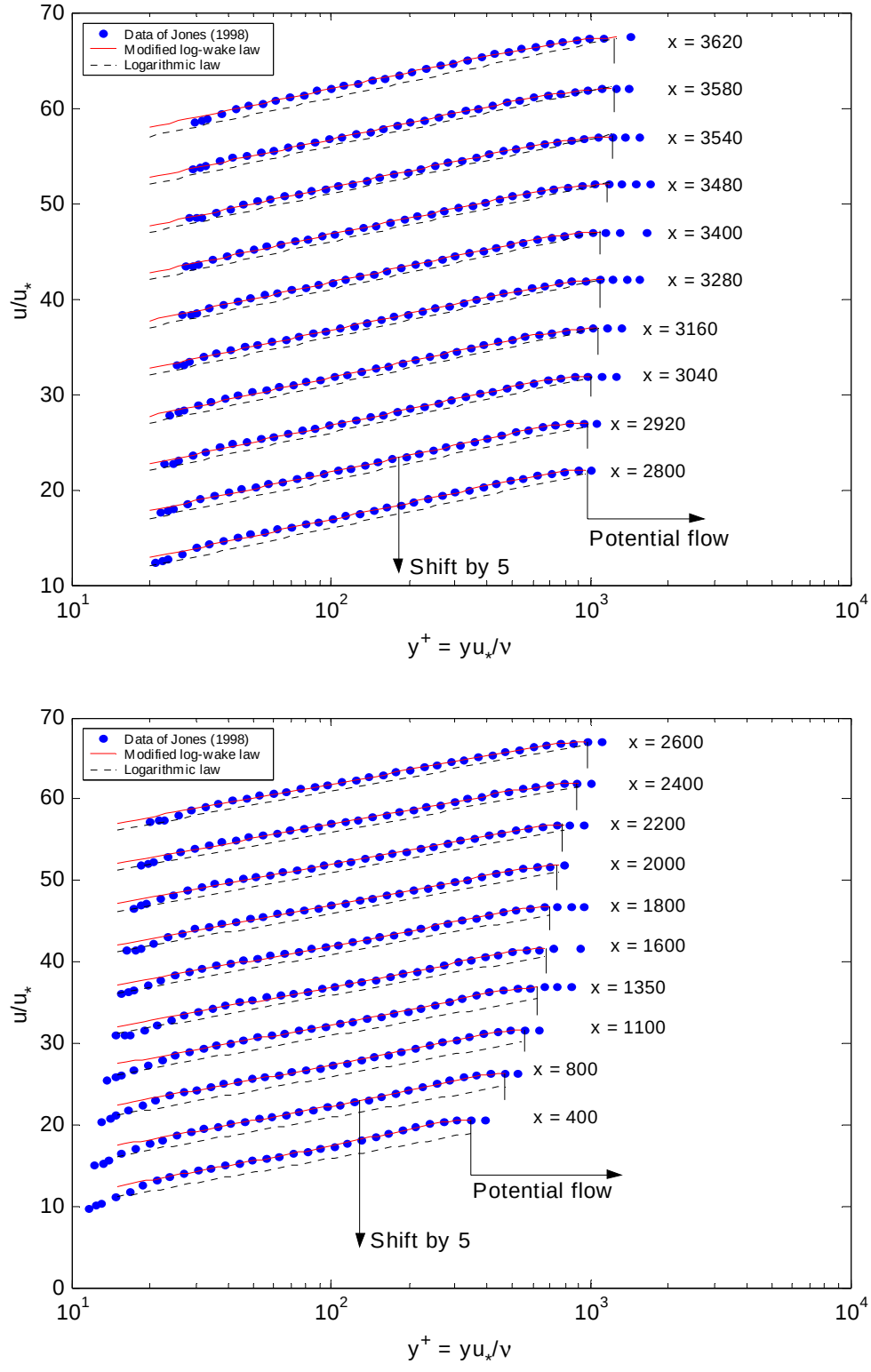

FIG. 4.2 Comparison of MLWL with Jones' experimental velocity profiles

($U = 5$ m/s, $K = 5.39\times10^{-7}$)

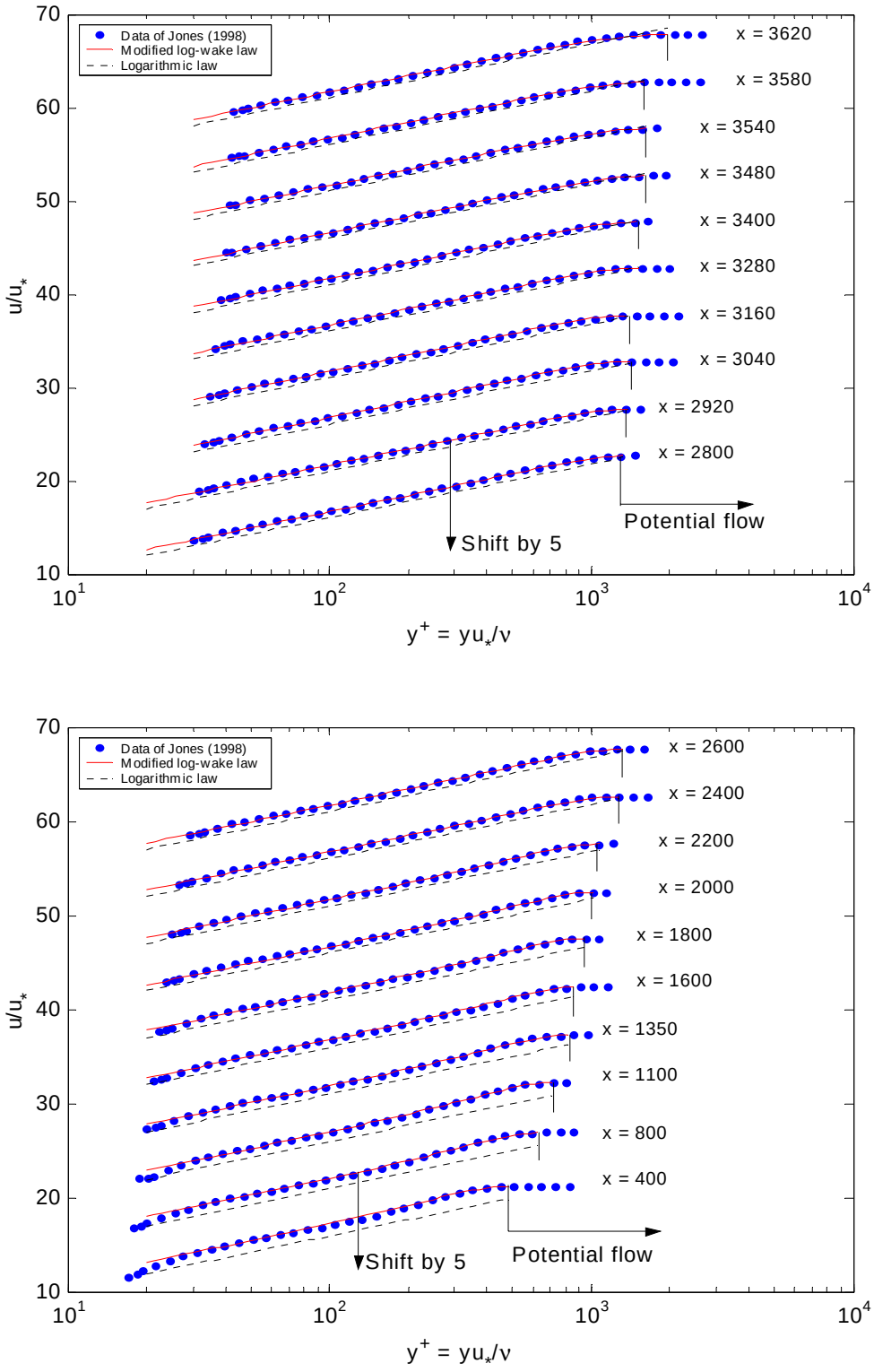

FIG. 4.3 Comparison of MLWL with Jones' experimental velocity profiles

($U = 7.5$ m/s, $K = 3.59\times10^{-7}$)

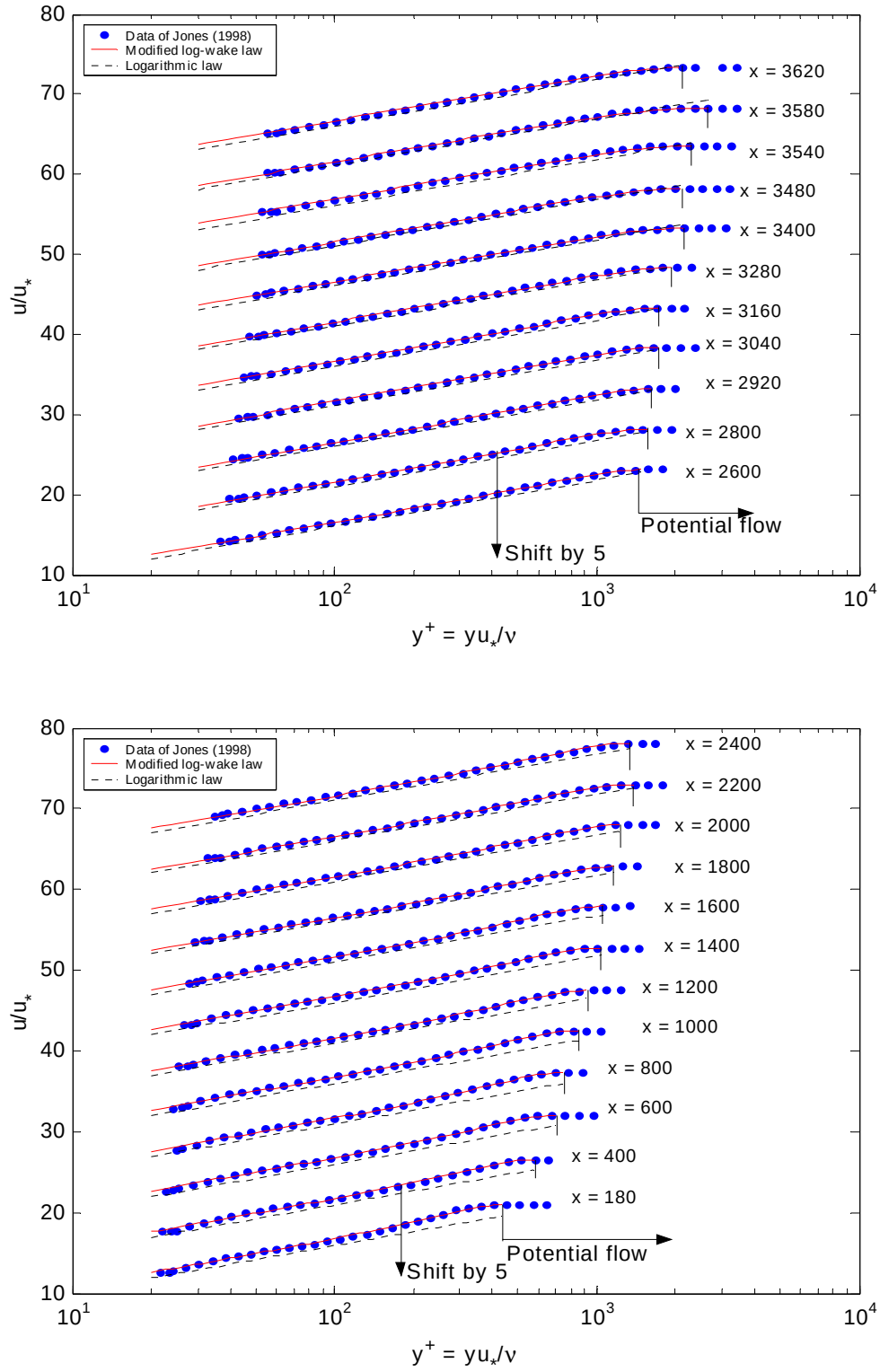

FIG. 4.4 Comparison of MLWL with Jones' experimental velocity profiles

($U = 10$ m/s, $K = 2.70\times10^{-7}$)

thickness δ could be calculated from (3.41), (3.42), and (3.60), respectively. With this method, the wall shear stress and boundary layer thickness can be defined in an experimental program. For simplification, only the skin friction factor c_f will be estimated to compare with experimental data in this thesis.

The predicting values of c_f of Jone's experiments by (3.63) are shown and compared with experimetal data in Tables 4.1 to 4.3.

Table 4.1 Basic data and parameters of Jones' experiments (U = 5 m/s, $K = 5.39\times10^{-7}$)

Station x (mm)	β	Π	Re_θ	c_f' Eq. 3.59	c_f data	$(c_f'-c_f)/c_f$ (%)
400	−0.1614	0.2218	630	0.005352	0.005244	2.0
800	−0.2417	0.2115	836	0.004994	0.004905	1.8
1100	−0.2797	0.1954	963	0.004843	0.004776	1.4
1350	−0.3233	0.1859	1090	0.004709	0.004623	1.8
1600	−0.3451	0.1755	1180	0.004632	0.004600	0.7
1800	−0.3630	0.1692	1229	0.004592	0.004565	0.6
2000	−0.3861	0.1572	1303	0.004541	0.004512	0.6
2200	−0.3986	0.1365	1351	0.004524	0.004506	0.4
2400	−0.4237	0.0792	1429	0.004519	0.004447	1.6
2680	−0.4407	0.0730	1520	0.004459	0.004391	1.5
2800	−0.4538	0.0740	1529	0.004452	0.004407	1.0
2920	−0.4609	0.0695	1549	0.004442	0.004394	1.1
3040	−0.4697	0.0495	1572	0.004444	0.004389	1.2
3160	−0.4812	0.0223	1610	0.004441	0.004377	1.4
3280	−0.5012	0.0141	1670	0.004409	0.004335	1.7
3400	−0.4975	0.0219	1669	0.004403	0.004355	1.1
3480	−0.5122	−0.0145	1699	0.004412	0.004342	1.6
3540	−0.5173	−0.0156	1713	0.004403	0.004331	1.6
3580	−0.5099	−0.0173	1712	0.004405	0.004331	1.7
3620	−0.5277	−0.0267	1784	0.004369	0.004304	1.5

Table 4.2 Basic data and parameters of Jones' experiments (U = 7.5 m/s, $K = 3.59\times10^{-7}$)

Station x (mm)	β	Π	Re_θ	c_f' (Eq. 3.60)	c_f (data)	$(c_f'-c_f)/c_f$ (%)
400	−0.1721	0.1939	883	0.004948	0.004817	2.6
800	−0.2422	0.2371	1163	0.004576	0.004498	1.7
1100	−0.2867	0.2521	1350	0.004399	0.004342	1.3
1350	−0.3127	0.2091	1477	0.004354	0.004292	1.4
1600	−0.3468	0.2147	1625	0.004252	0.004231	0.5
1800	−0.3674	0.2037	1715	0.004211	0.004177	0.8
2000	−0.3842	0.1690	1799	0.004198	0.004156	1.0
2200	−0.4066	0.1617	1903	0.004151	0.004130	0.5
2400	−0.4279	0.0757	1998	0.004179	0.004091	2.1
2680	−0.4256	0.0715	2055	0.004155	0.004085	1.7
2800	−0.4510	0.0755	2117	0.004124	0.004076	1.2
2920	−0.4577	0.0579	2150	0.004123	0.004071	1.3
3040	−0.4709	0.0522	2217	0.004098	0.004051	1.1
3160	−0.4754	0.0550	2230	0.004091	0.004053	0.9
3280	−0.4983	0.0324	2326	0.004068	0.004012	1.4
3400	−0.4910	0.0286	2311	0.004077	0.004049	0.7
3480	−0.4946	−0.0032	2329	0.004091	0.004047	1.1
3540	−0.5029	−0.0044	2372	0.004075	0.004025	1.2
3580	−0.4992	−0.0209	2348	0.004094	0.004041	1.3
3620	−0.5267	−0.0916	2460	0.004089	0.003985	2.5

As shown in Tables 4.1, 4.2 and 4.3, the largest relative error of skin friction factor c_f is 2.9%, equation (3.63) agrees with the experimental data fairly well. The excellent agreement validates the modified log-wake law not only for velocity profiles but also for the skin friction factor.

Table 4.3 Basic data and parameters of Jones' experiments (U = 10 m/s, $K = 2.70\times10^{-7}$)

Station x (mm)	β	Π	Re_θ	c_f' (Eq. 3.60)	c_f (data)	$(c_f'-c_f)/c_f$ (%)
180	−0.1313	0.3148	855	0.004828	0.004720	2.2
400	−0.1766	0.2858	1122	0.004556	0.004508	1.1
600	−0.2123	0.2605	1314	0.004419	0.004340	1.8
800	−0.2417	0.3056	1466	0.004256	0.004221	0.8
1000	−0.2670	0.2642	1616	0.004206	0.004160	1.1
1200	−0.2896	0.2467	1745	0.004150	0.004109	1.0
1400	−0.3143	0.2161	1888	0.004106	0.004051	1.3
1600	−0.3435	0.2164	2039	0.004035	0.003985	1.2
1800	−0.3628	0.2170	2150	0.003986	0.003961	0.6
2000	−0.3896	0.1735	2299	0.003993	0.003906	2.2
2200	−0.4102	0.1555	2411	0.003939	0.003887	1.3
2400	−0.4174	0.1496	2489	0.003916	0.003890	0.7
2600	−0.4355	0.1433	2574	0.003892	0.003968	−2.0
2800	−0.4527	0.1202	2683	0.003875	0.003844	0.8
2920	−0.4635	0.1081	2728	0.003870	0.003828	1.1
3040	−0.4800	0.0947	2819	0.003851	0.003792	1.5
3160	−0.4872	0.0929	2832	0.003848	0.003789	1.5
3280	−0.5061	0.0477	2946	0.003847	0.003788	1.5
3400	−0.5013	−0.0226	2987	0.003878	0.003814	1.7
3480	−0.5082	−0.0155	3026	0.003863	0.003788	1.9
3540	−0.5170	−0.0630	3032	0.003887	0.003793	2.4
3580	−0.5214	−0.1241	3100	0.003892	0.003780	2.9
3620	−0.5112	−0.1570	3029	0.003862	0.003811	1.3

4.4 TEST WITH IVAN MARUSIC'S EXPERIMENTAL DATA (APG)

4.4.1 BASIC INFORMATION OF MARUSIC'S EXPERIMENTS

The 12 adverse pressure gradient (APG) experimental velocity profiles by Ivan Marusic can be found on the website http://www.mame.mu.oz.au/~ivan/index.html. These are the

results from experiments in adverse pressure gradient boundary layers as reported by Perry and Marusic (1995), Marusic and Perry (1995). The description of apparatus and other basic information can be found in the website and their published papers (1995).

4.4.2 VELOCITY PROFILES

The experimental data are at 2 levels of upstream velocity: 10 m/s and 30 m/s. The boundary layers are measured in 6 stations from x = 1200 to 3080 mm for each flow case. The comparison of experimental boundary layers with the MLWL (4.1) is shown in Figs. 4.5 to 4.6. One can note that the MLWL agrees with the experimental data precisely. The same conclusion as in Section 4.3 can be received.

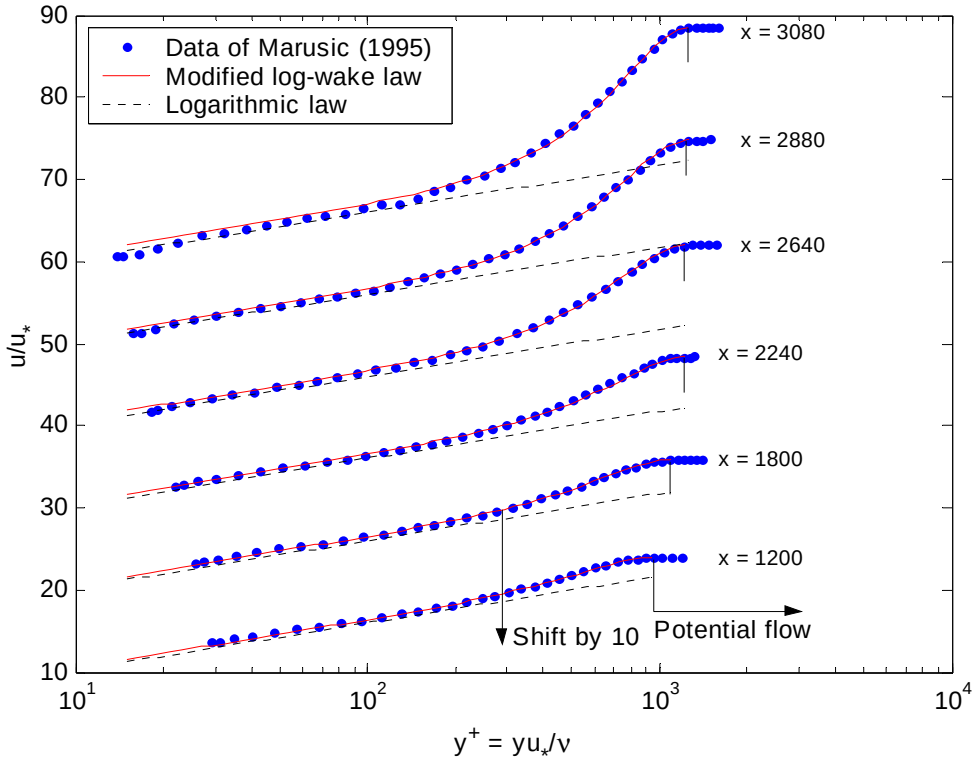

FIG. 4.5 Comparison of MLWL with Masuric's experimental velocity profiles (U = 10 m/s)

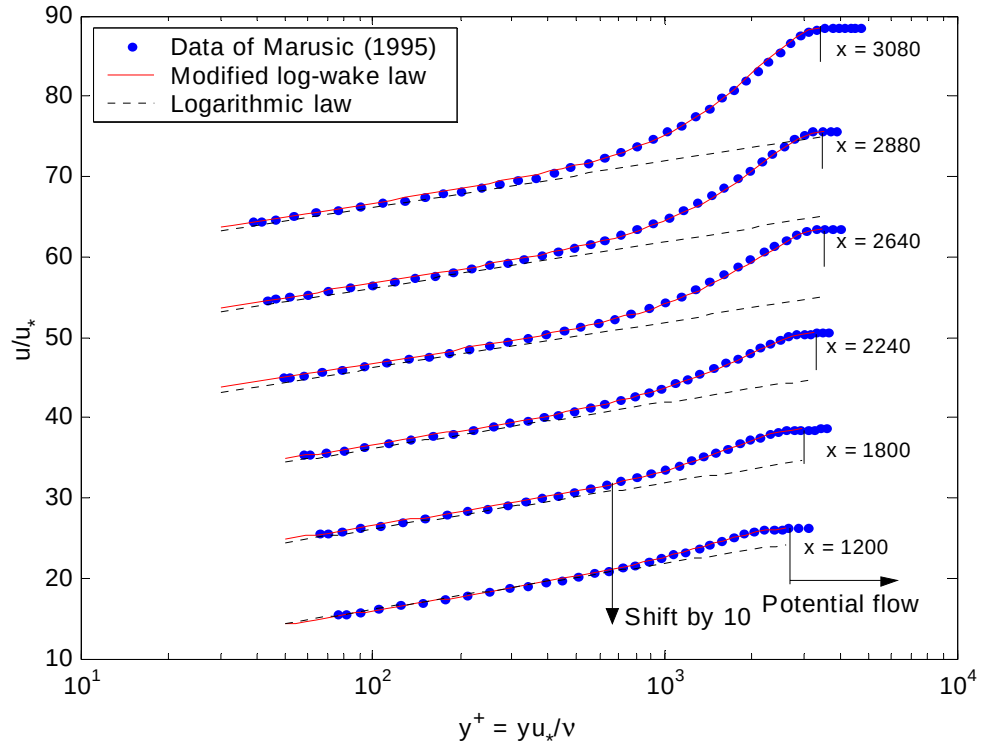

FIG. 4.6 Comparison of MLWL with Masuric's experimental velocity profiles ($U = 30$ m/s)

The parameter Π gained in the curve fit process for each velocity profile is shown in Tables 4.4 to 4.5. The correclation of Π with β will be treated with other experimental data in Section 4.11.

4.4.3 SKIN FRICTION FACTOR c_f

Following the procedure introduced in § 4.3.3 step bye step, the value of skin friction factor c_f predicted by the MLWL could be gained and shown with experimental data in Tables 4.4 to 4.5.

Table 4.4 Basic data and parameters of Marusic's experiments (U = 10 m/s)

Station x (mm)	β	Π	Re_{θ}	c_f' (Eq. 3.60)	c_f (data)	$(c_f'-c_f)/c_f$ (%)
1200	0.00	0.5604	2206	0.003621	0.003604	0.5
1800	0.65	0.8579	3153	0.003087	0.003094	−0.2
2240	1.45	1.2918	4156	0.002582	0.002540	1.6
2640	2.90	1.9955	5395	0.002021	0.002011	0.5
2880	4.48	2.5575	6359	0.001699	0.001680	1.1
3080	7.16	3.2424	7257	0.001405	0.001370	2.5

Table 4.5 Basic data and parameters of Marusic's experiments (U = 30 m/s)

Station x (mm)	β	Π	Re_{θ}	c_f' (Eq. 3.60)	c_f (data)	$(c_f'-c_f)/c_f$ (%)
1200	0.00	0.5846	6431	0.002895	0.002872	0.8
1800	0.71	0.8767	8588	0.002542	0.002509	1.3
2240	1.39	1.2134	10997	0.002227	0.002206	0.9
2640	2.74	1.7381	14209	0.001863	0.001850	0.7
2880	3.96	2.1985	16584	0.001621	0.001619	0.1
3080	6.07	2.7777	19133	0.001381	0.001380	0.1

Tables 4.4 and 4.5 show the largest relative error of skin friction factor c_f is 2.5%, equation (3.63) agree with the experimental data fairly well. Again, the excellent agreement validates the modified log-wake law not only for velocity profiles but also for the skin friction factor.

4.5 TEST WITH A. E. SAMUEL'S EXPERIMENTAL DATA (APG)

4.5.1 BASIC INFORMATION OF SAMUEL'S EXPERIMENTS

Samuel's experimental data are presented on the website for the databank of Journal of Fluid Engineering: http://scholar.lib.vt.edu/ejournals/JFE/data/JFE/DB96-243/d4/f0141a. The details of experimental equipments and the results were reported by Samuel and Joubert (1974). These data consist of 12 APG experimental velocity profiles in turbulent boundary layers developing on a smooth wall in an adverse pressure gradient domain.

4.5.2 VELOCITY PROFILES

The boundary layer velocity profiles of Samuel's experiments are measured in 12 stations from x = 855 to 3400 mm. The comparison of experimental boundary layers with the MLWL (4.1) is shown in Fig. 4.7. One can note that the MLWL agrees with the experimental data precisely. The same conclusion as in Section 4.3 can be received.

The parameter Π gained in the curve fit process for each velocity profile is shown in Table 4.6. The correclation of Π with β will be treated with other experimental data in Section 4.11.

4.5.3 SKIN FRICTION FACTOR c_f

The value of kinematic viscosity for each boundary layer measured in Samuel's experiments is not available. Howerver, it's so difficult to find suitable experimental data for this study, a constant value of kinematic viscousity for all boundary layer was assumed by common sense, i.e. $\nu = 1.5159 \times 10^{-5}$ m^2/s. With this value of kinematic viscosity,

following the procedure introduced in §4.3.3 step bye step, the value of skin friction factor c_f predicted by the MLWL could be gained and shown with experimental data in Table 4.6.

The largest relative error of skin friction factor c_f calculated form (3.63) is 5.1% shown in Table 4.6. Even though the assumption of the constant value of kinetic viscosity was used, equation (3.63) still agrees with the experimental data well. Again, the excellent agreement validates the modified log-wake law not only for velocity profiles but also for the skin friction factor.

Table 4.6 Basic data and parameters of Samuel's experiments

Station x (mm)	β	Π	Re_θ	c_f' (Eq. 3.60)	c_f (data)	$(c_f'-c_f)/c_f$ (%)
855	0.09	0.7637	4904	0.002909	0.002760	5.1
1160	0.14	0.7740	5803	0.002831	0.002700	4.6
1440	0.22	0.8784	6514	0.002672	0.002600	2.7
1760	0.32	0.8910	7152	0.002618	0.002550	2.6
2100	0.53	0.9446	8520	0.002500	0.002400	4.0
2260	0.67	1.0008	9078	0.002435	0.002370	2.7
2400	0.91	1.0949	9498	0.002356	0.002260	4.1
2560	1.47	1.3197	10742	0.002174	0.002100	3.4
2720	2.32	1.4517	12007	0.002061	0.002000	3.0
2870	2.90	1.6951	12525	0.001921	0.001880	2.1
3040	3.88	2.0060	13671	0.001750	0.001700	2.9
3400	7.72	3.1337	18124	0.001281	0.001250	2.4

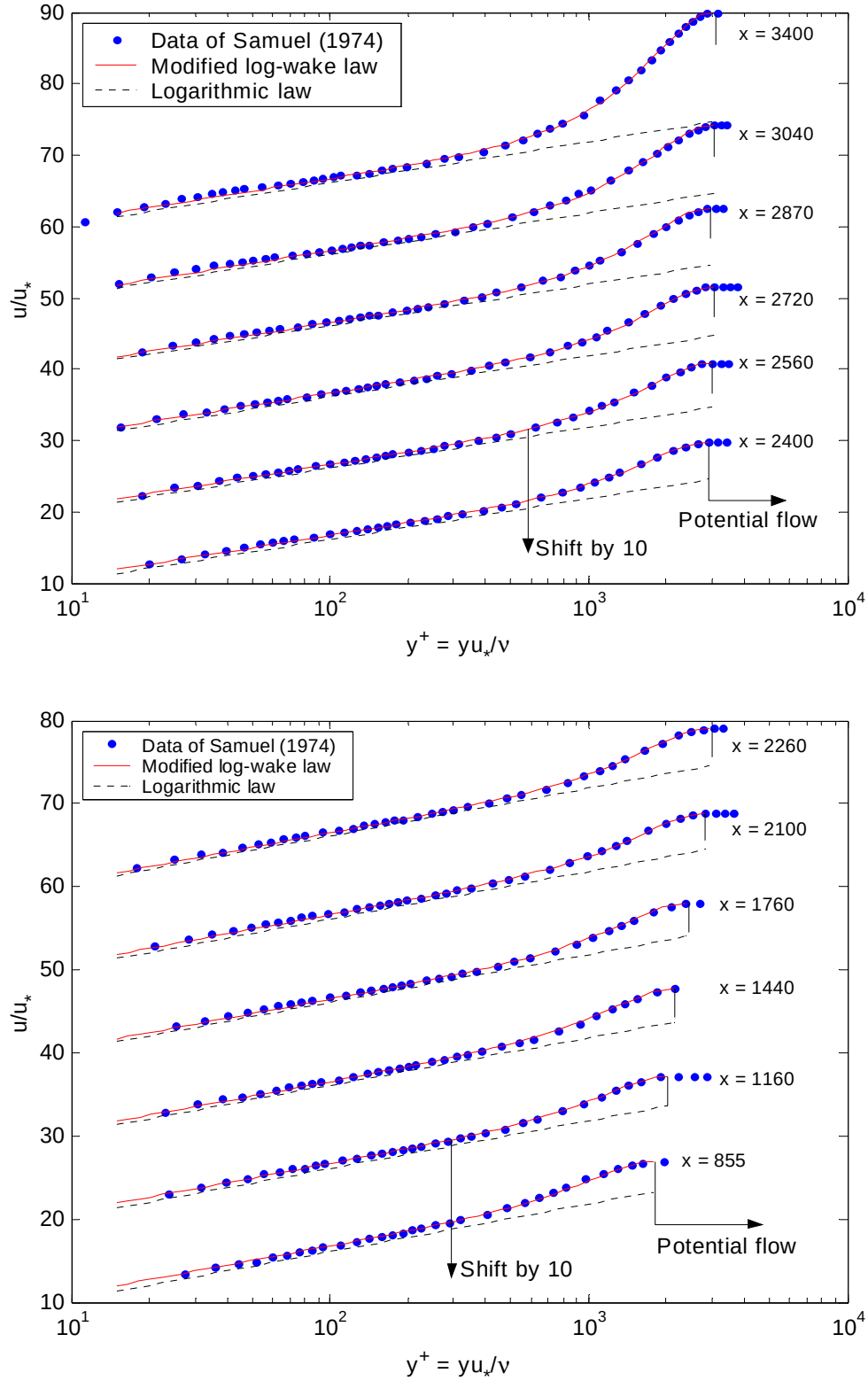

FIG. 4.7 Comparison of MLWL with Samuel's experimental velocity profiles

4.6 TEST WITH YASUTAKA NAGANO'S EXPERIMENTAL DATA (APG)

4.6.1 BASIC INFORMATION OF NAGANO'S EXPERIMENTS

Nagano et al. conducted experiments to study the structure of turbulent boundary layer subjected to adverse pressure gradient in 1992 and 1998. Each experiment contained 4 and 5 velocity profiles of APG boundary layers, respectively. The same experimental apparatus is used. The equipments and instruments were introduced by Nagano et al. (1992). Consequently, this section will discuss both of these two series of boundary layers.

4.6.2 VELOCITY PROFILES

The boundary layer velocity profiles of Nagano's experiments were measured in 4~5 stations from x = 523 to 1121 mm. The comparison of each experimental boundary layer with the MLWL (4.1) is shown in Fig. 4.8. One can note that the MLWL agrees with the experimental data precisely. The same conclusion as in Section 4.3 can be received.

The parameter Π gained in the curve fit process for each velocity profile is shown in Tables 4.7 and 4.8 The correclation of Π with β will be treated with other experimental data in Section 4.11.

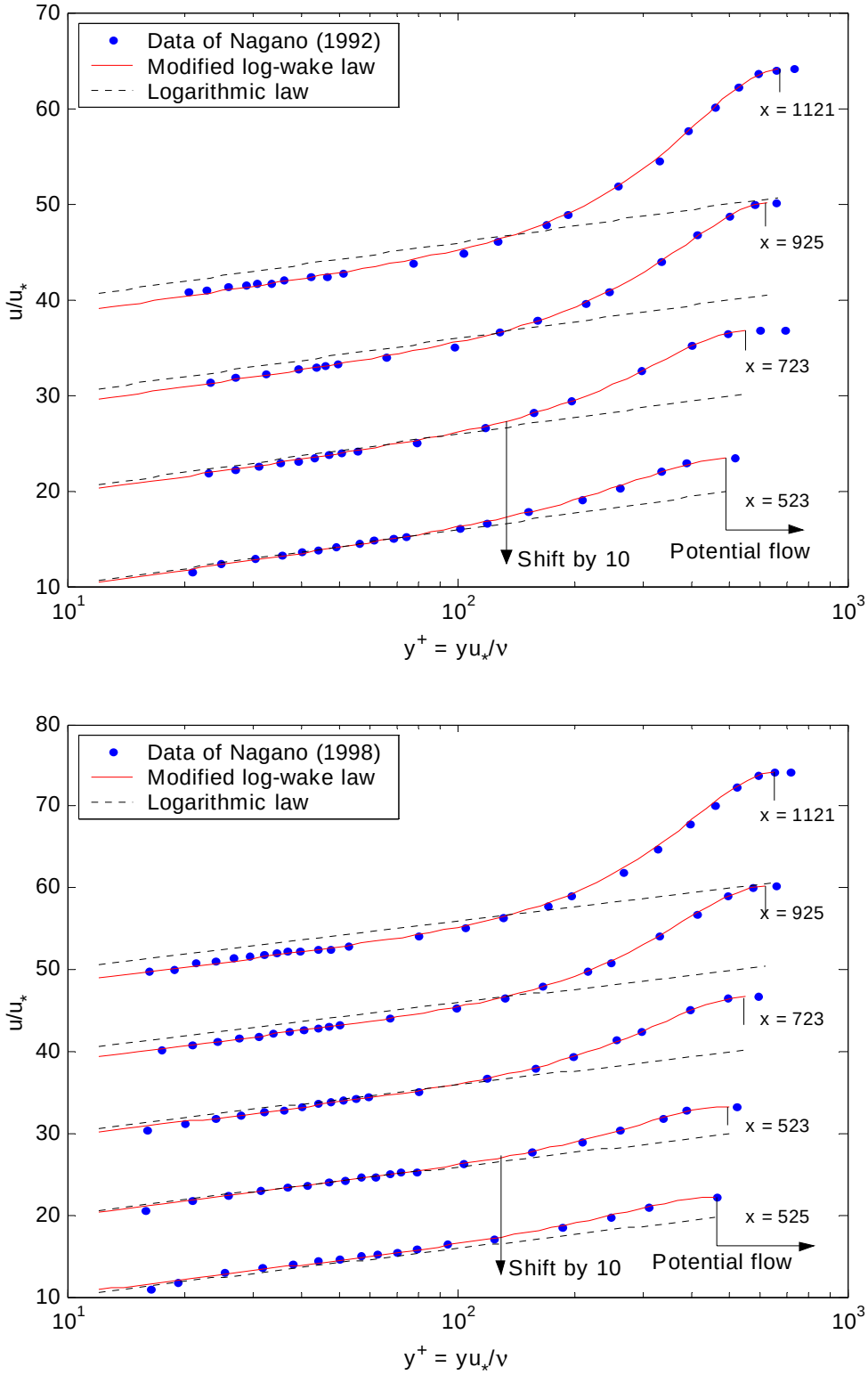

FIG. 4.8 Comparison of MLWL with Nagano's experimental velocity profiles

4.6.3 SKIN FRICTION FACTOR c_f

Following the procedure introduced in §4.3.3 step bye step, the value of skin friction factor c_f predicted by the MLWL could be gained and shown with other experimental data in Tables 4.7 and 4.8..

From Tables 4.7 and 4.8, one can see the largest relative error of skin friction factor c_f is 8.1%, equation (3.63) agrees with the experimental data not bad. Again, the agreement validates the modified log-wake law not only for velocity profiles but also for the skin friction factor.

Table 4.7 Basic data and parameters of Nagano's experiments (1992)

Station x (mm)	β	Π	Re_θ	c_f' (Eq. 3.60)	c_f (data)	$(c_f'-c_f)/c_f$ (%)
523	0.77	0.872	1290	0.00367	0.00369	-4.8
723	2.19	1.562	1880	0.00274	0.00282	-2.7
925	3.95	2.357	2660	0.00209	0.00222	-5.8
1121	5.32	3.154	3350	0.00159	0.00174	-8.5

Table 4.8 Basic data and parameters of Nagano's experiments (1998)

Station x (mm)	β	Π	Re_θ	c_f' (Eq. 3.60)	c_f (data)	$(c_f'-c_f)/c_f$ (%)
525	0.00	0.557	1070	0.00422	0.00397	6.3
523	0.76	0.890	1290	0.00369	0.00369	0.0
723	2.05	1.573	1880	0.00275	0.00282	-2.5
925	3.54	2.289	2660	0.00205	0.00222	-7.7
1121	4.66	3.166	3350	0.00160	0.00174	-8.1

4.7 TEST WITH P. E. SKARE'S EXPERIMENTAL DATA (APG)

4.7.1 BASIC INFORMATION OF SKARE'S EXPERIMENTS

The experimental results for an equilibrium boundary layer in a strong adverse pressure gradient flow are reported by Skare and Krogstad (1994). The experimental details also were described in their published paper (Skare and Krogstad, 1994).

4.7.2 VELOCITY PROFILES

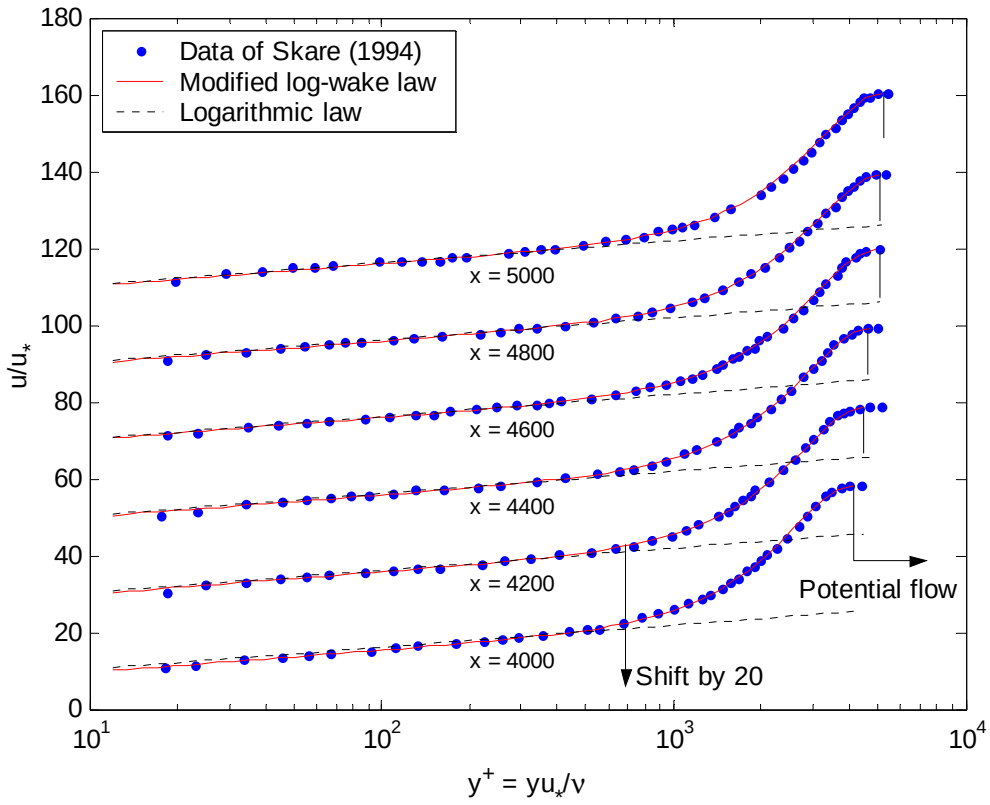

FIG. 4.9 Comparison of MLWL with Skare's experimental velocity profiles

The streamwise mean velocity profiles of the APG boundary layer flow were measured in 12 stations from x = 3000 to 5200 mm. Only the data of six boundary layers, say the stations x = 4000, 4200, 4400, 4600, 4800, and 5000 mm, are available. The comparison of each experimental boundary layer with the MLWL (4.1) is shown in Fig. 4.9. One can note that the MLWL agrees with the experimental data precisely. The same conclusion as in Section 4.3 can be received.

The parameter Π gained in the curve fit process for each velocity profile is shown in Table 4.9. The correclation of Π with β will be treated with other experimental data in Section 4.11.

4.7.3 SKIN FRICTION FACTOR c_f

Following the procedure introduced in §4.3.3 step bye step, the value of skin friction factor c_f predicted by the MLWL could be gained and shown with other experimental data in Table 4.9.

Table 4.9 Basic data and parameters of Skare's experiments

Station x (mm)	β	Π	Re_θ	c_f' (Eq. 3.60)	c_f (data)	$(c_f'-c_f)/c_f$ (%)
4000	19.9	6.85	39120	0.000577	0.000590	−2.2
4200	20.0	6.88	41580	0.000579	0.000582	−0.5
4400	19.6	6.93	44420	0.000564	0.000585	−3.6
4600	20.1	6.90	46250	0.000565	0.000571	−1.1
4800	20.2	6.91	49180	0.000561	0.000567	−1.1
5000	21.2	7.06	50980	0.000546	0.000546	0.0

Table 4.9 shows the largest relative error of skin friction factor c_f is 3.6%, equation (3.63) agrees with the experimental data very well. Again, the agreement validates the modified log-wake law not only for velocity profiles but also for the skin friction factor.

4.8 TEST WITH ALBERTO AYALA'S EXPERIMENTAL DATA (APG)

4.8.1 BASIC INFORMATION OF AYALA'S EXPERIMENTS

Ayala's experiments were considered for mild ($\beta = 0.8$, $\mathrm{Re}_\theta = 3500$) and moderate ($\beta = 1.8$, $\mathrm{Re}_\theta = 3790$) adverse-pressure-gradient conditions. The base case for zero-pressure-gradient condition ($\beta = 0$, $\mathrm{Re}_\theta = 2681$) was also investigated. The experimental details were described in their published paper (Ayala et al., 1999).

4.8.2 VELOCITY PROFILES

The comparison of each experimental boundary layer with the MLWL (4.1) is shown in Fig. 4.10. One can note that the MLWL agrees with the experimental data precisely. The same conclusion as in Section 4.3 can be received.

The parameter Π gained in the curve fit process for each velocity profile is shown in Table 4.10. The correclation of Π with β will be treated with other experimental data in Section 4.11.

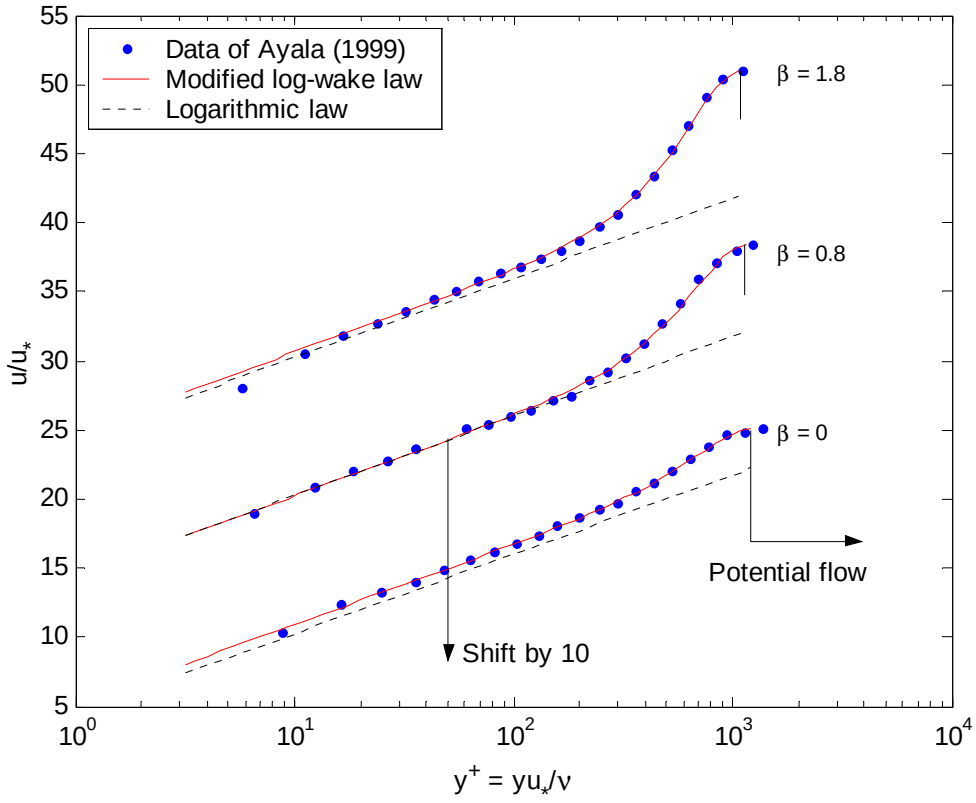

FIG. 4.10 Comparison of MLWL with Ayala's experimental velocity profiles

4.8.3 SKIN FRICTION FACTOR c_f

Following the procedure introduced in § 4.3.3 step bye step, the values of skin friction factor c_f predicted by the MLWL could be gained and shown with other experimental data in Table 4.10.

Table 4.10 shows the largest relative error of skin friction factor c_f is 7.5%, equation (3.63) agrees with the experimental data well. Again, the agreement validates the modified log-wake law not only for velocity profiles but also for the skin friction factor.

Table 4.10 Basic data and parameters of Ayala's experiments

No.	β	Π	Re_θ	c_f' (Eq. 3. 60)	c_f (data)	$(c_f'-c_f)/c_f$ (%)
1	0.0	0.60	2681	0.003439	0.003200	7.5
2	0.8	1.43	3500	0.002554	0.002490	2.6
3	1.8	1.89	3790	0.002207	0.002080	6.1

4.9 TEST WITH H. J. HERRING'S EXPERIMENTAL DATA (FPG)

4.9.1 BASIC INFORMATION OF HERRING'S EXPERIMENTS

Herring et al. built a wind tunnel for boundary-layer studies in which an arbitrary negative pressure gradient could be developed. The experimental results and the apparatus were reported in their published paper (Herring and Norbury, 1967).

4.9.2 VELOCITY PROFILES

The comparison of each experimental boundary layer with the MLWL (4.1) is shown in Fig. 4.11. One can note that the MLWL agrees with the experimental data excellently. The same conclusion as in Section 4.3 can be received.

The parameter Π gained in the curve fit process for each velocity profile is shown in Table 4.11. The correclation of Π with β will be treated with other experimental data in Section 4.11.

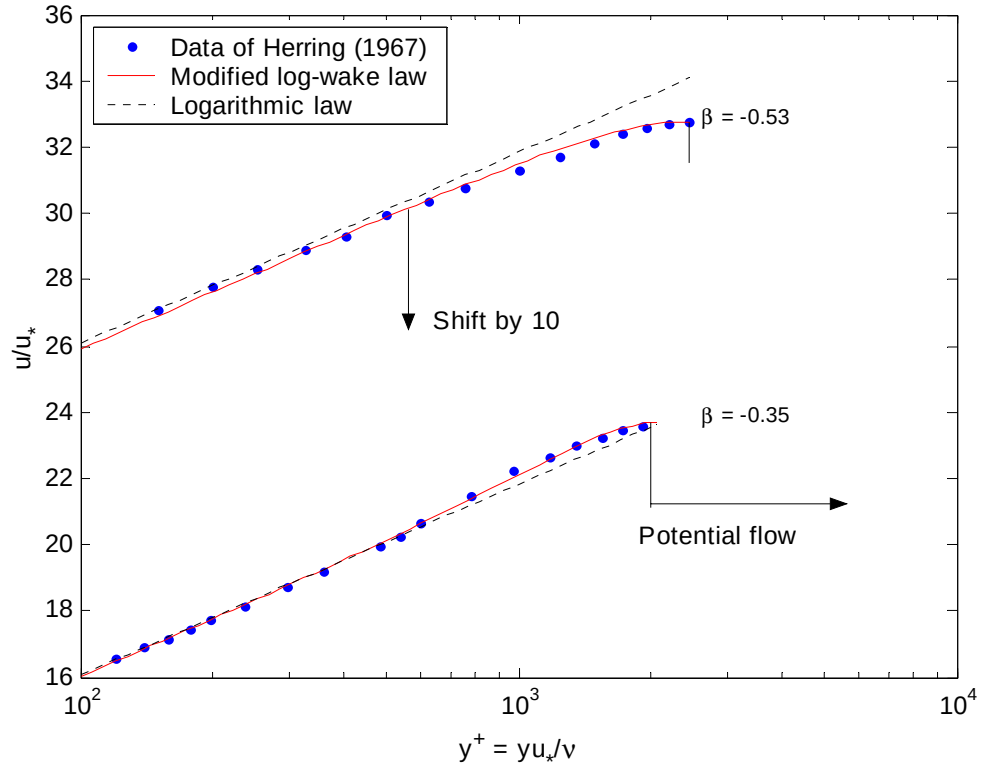

FIG. 4.11 Comparison of MLWL with Herring's experimental velocity profiles

Table 4.11 Basic data and parameters of Herring's experiments

No.	β	Π
1	-0.35	0.188
2	−0. 53	-0.059

The experimental data of skin friction factor c_f are not available, so the comparison of predicted c_f with experimental c_f can not be done in this Section.

4.10 TEST WITH F. CLAUSER'S EXPERIMENTAL DATA (APG)

4.10.1 BASIC INFORMATION OF CLAUSER'S EXPERIMENTS

The experimental results and the apparatus were reported in Clauser's published paper (1954).

4.10.2 VELOCITY PROFILES

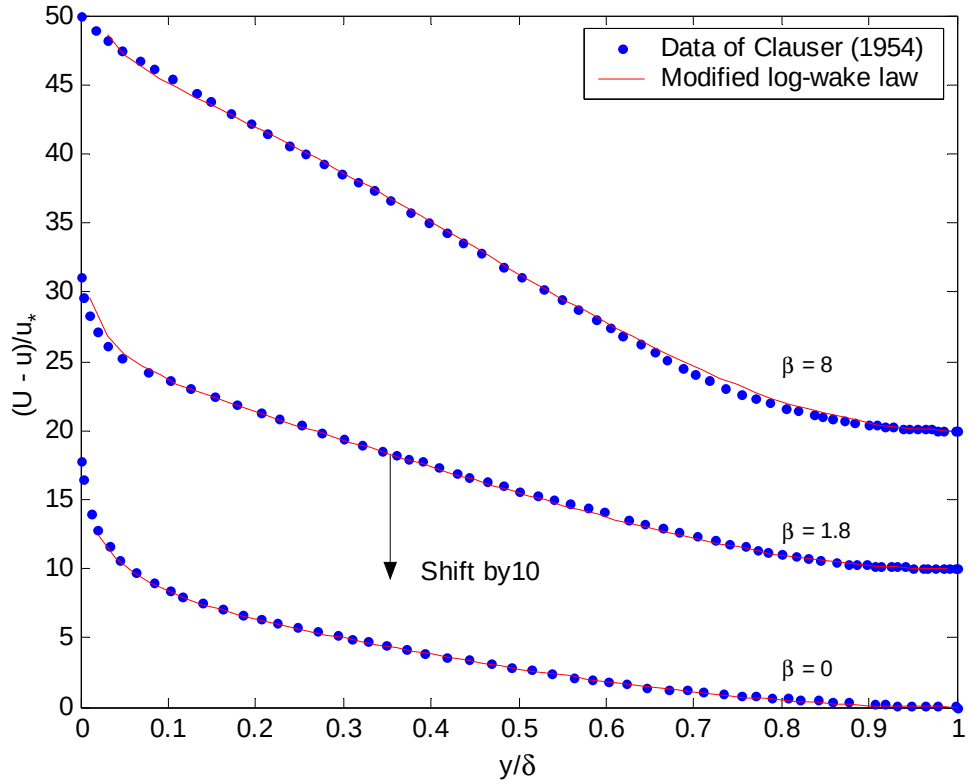

FIG. 4.12 Comparison of MLWL with Clauser's experimental velocity profiles

The experimental data were gained in the velocity defect form, so the defect form of the MLWL (3.38) is employed to test the MLWL. The comparison of each experimental boundary layer with the MLWL defect form (3.38) is shown in Fig. 4.12. One can note that the MLWL agrees with the experimental data precisely. The same conclusion as in Section 4.3 can be received.

The parameter Π gained in the curve fit process for each velocity profile is shown in Table 4.12. The correclation of Π with β will be treated with other experimental data in Section 4.11.

Table 4.12 Basic data and parameters of Clauser's experiments

No.	β	Π
1	0.0	0.722
2	1.8	1.826
3	8. 0	4.123

The experimental data of skin friction factor c_f are not available, so the comparison of predicted c_f with experimental c_f can not be done in this Section.

4.11 CORRELATION OF Π WITH β

As previously mentioned, the Coles' wake strength Π reflects the effects of pressure gradient on boundary layer velocity distribution. The intensity of pressure gradient is usually represented by the Clauser pressure gradient parameter $\beta = (\delta^* / \tau_w) dp/dx$. A relationship of Π and β could be set up to predict the value of Π when a boundary layer is measured. Based on the log-wake law (2.4), Das (1987) summed up a second-order polynomial to express the correlation of Π with β (2.4). Similarly, a second-order polynomial is employed to describe the correlation of Π with β based on the modified log-wake law (2.5) in this study.

In section 4.3 to 4.10, a value of Π and a value of β were gained and presented in Table 4.1 to 4.12 for each boundary layer velocity profile. A least-squares curve fitting reveals that the relationship of Π and β can express as

$$\Pi = -0.0105\beta^2 + 0.535\beta + 0.40 \tag{4.4a}$$

$$\beta = 0.25\Pi^2 + 1.28\Pi - 0.59 \tag{4.4b}$$

The data of β versus Π gained in the previous sections, equations (4.4) and (2.6) are plotted in Figure 4.13. One can see the difference between Equation (4.4) and (2.6) induced by the cubic correction term is not large. Equation (4.4) can be regarded as a modified version of Equation (2.6).

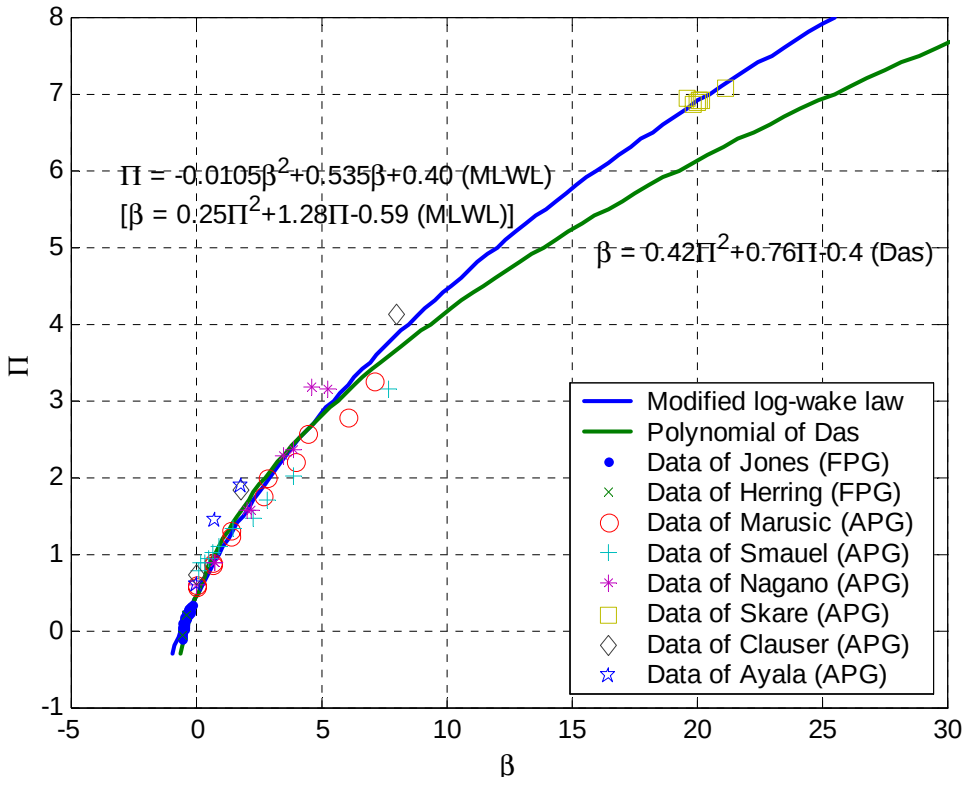

Figure 4.13 Correlation of the wake strength with the Clauser pressure gradient parameter

4.12 SUMMARY

The experimental data used in this chapter were produced in different laboratory and at different time, but all of them agree with MLWL quite well not only for the velocity profile but also for the skin friction factor. The MLWL is valid for turbulent flat plate boundary layers under zero, favorable or adverse pressure gradient. The following conclusions can be summarized:

a) The basic structure of the MLWL is correct;

b) The MLWL is suitabel to simulate the turbulent NPG flat plate boundary layers;

c) The MLWL can replicate the experimental data from the overlap ragion till the boundary layer edge, i.e., $30 \le yu_* / \nu$ and $\xi = y/\delta = \left(yu_* / \nu\right)/\mathrm{Re}_\delta \le 1$;

d) The MLWL tends to a straight line in a semilog plot in the overlap region and then concides with the logarithmic law;

e) The zero velocity gradient at the boundary layer edge can be clearly seen from all profiles in Figures 4.2 to 4.12 which imply that the boundary correction is necessary.

f) The friction factor derived from the modified log-wake law is accurate in terms of the momentum thickness. The prediction of skin friction factor c_f and wall shear stress τ_w of boundary layer can be performed by Equantio (3.63), and (3.41).

g) Based on MLWL, the Coles' wake strength Π can be predicted by (4.4)

CHAPTER FIVE

PATCH TEST OF FLUENT FOR NUMERICAL EXPERIMENT OF OPEN-CHANNEL FLOW

5.1 INTRODUCTION

Some patch tests were conducted in this chapter to assure that the CFD computer program software – FLUENT is suitable for the numerical experiments of open-channel flows which will be performed in next chapter. At the same time, the setup designs of numerical experiments also were inspected.

The open-channel flow is one of the very important fundaments of hydraulic engineering. Although it seems quite simple, but its numerical simulation is still a hotspot for research until the present time. All the experimental data available of open-channel flows were taken from the 3D experiments. In order to make the numerical simulation results could compare to the experimental data reasonably, the patch tests should be done as 3D problems. The difficulties of the numerical simulation lie on two aspects, one is damping influence of the free surface, another is the turbulence-driven secondary motion. In this

thesis, the Volume of Fluid (VOF) multiphase model is employed to simulate the interaction on the free surface between the water and air, and the Reynolds Stress Model (RSM) to predict the turbulence-driven secondary flows.

At first, the patch test in Section 5.2 qualitatively shows that the Reynolds Stress Model in FLUENT is capable to predict the secondary current very well. Secondly, the capability of FLUNT to simulate three dimension open-channel flows is tested in Section 5.2. Finally, a summary of this chapter is given in Section 5.4.

5.2 PATCH TEST OF SECONDARY FLOW IN SQUARE TUBE

It is an unfortunate fact that no single turbulence model is universally accepted as being superior for all classes of problems. FLUENT provides five kinds of turbulent models for choice, i.e. the Spalart-Allmaras model, the $k-\varepsilon$ model, the $k-\varpi$ model, the Reynolds stress model and the large eddy simulation model. Cokljat and Younis (1995) recommended the Reynolds stress model to predict the secondary motion and the effects of free surface. So, the Reynolds stress model was employed in all numerical simulation in this thesis

A straight square tube flow was used to check the capability of simulating secondary flow for FLUENT. The sketch of model setup is shown in Figure 5.1. Wang et al. (1994) pointed out the fully-developed state occurred at a downstream location of $x/D_h \geq 80$, in which x is the streamwise coordinate, D_h denotes the hydraulic diameter of square tube.

The hydraulic diameter is 0.5m in this case, so the length of tube was chosen as 50 m. The other flow parameters are listed in Table 5.1.

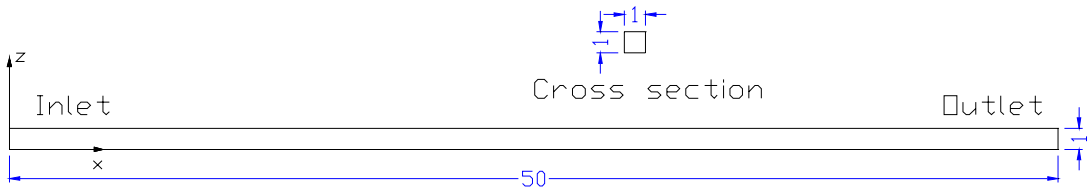

Figure 5.1 Side view and cross section of square tube (unit: m)

Table 5.1 Basic conditions and parameters of square tube flow

Material	Water		Inlet velocity, U (m)	0.1004 m/s
Length, (m)	50		Outlet condition	$\frac{\partial u}{\partial x} = 0$
Size of cross section, (m)	1 × 1		Wall condition	No slip
Hydraulic diameter, D_h (m)	0.5		Gravity force	Neglected
Viscous model	Reynolds stress model		$\mathrm{Re} = \frac{UD_h}{\nu}$	50000

Figures 5.2 and 5.3 qualitatively show a typical distribution of primary velocity and a typical distribution of secondary flow vectors which can be found in many literatures (Wang et al., 1994, Nezu and Nakagawa, 1993, p.102), respectively. It is no doubt that FLUENT is capable to predict the secondary flow in open channel successfully. In this section, we do not concern on the magnitude of the characteristics of square tube flow. The test about magnitude will be conducted in next section.

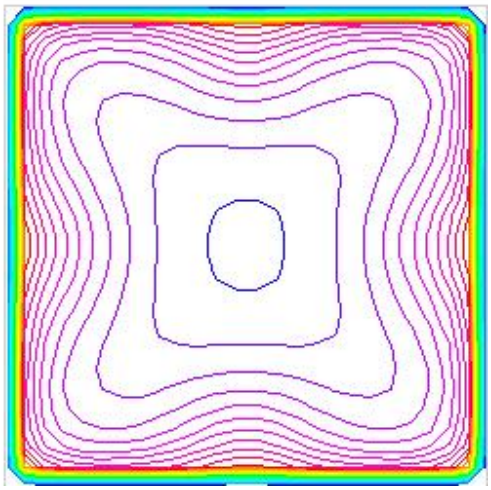

Figure 5.2 Contour lines of mean primary velocity at section x = 48 m

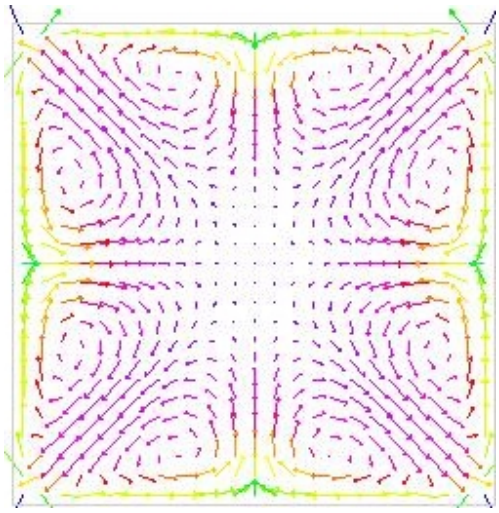

Figure 5.3 Vector descriptions of secondary flows at section x = 48 m

5.3 PATCH TEST OF 3D OPEN-CHANNEL FLOW

The simulation of one run of Lyn's experiments was made as a patch test to identify whether FLUENT could be or not employed to perform the numerical experiments of open-channel flows.

5.3.1 LYN'S EXPERIMENTAL DATA IN OPEN CHANNEL

Lyn's experiments were carried out at Caltech and the velocities were measured using a Laser-Doppler-Velocimeter (LDV). The experimental description can be found in several documents (Lyn, 1986, 2000, Guo and Julien, 2002). The experiments were performed in a smooth rectangular flume with 13 m long and 26.7 cm wide. The flow characteristics of run C2 chosen to be simulated from the four reported clear water runs are tabulated in Table 5.2.

Table 5.2 Flow characteristics for run C2 of Lyn's experiments

Data set	C2		Average velocity U (m/s)	0.772
Slope, S	0.0027		Maximum velocity, u_{max}, (m/s)	0.874
Depth, h (m)	0.0653		Width, w (m)	0.267
Hydraulic radius, R_h (m)	4.38		Boundary layer thickness, δ (m)	0.0523
Reynolds number, $\mathrm{Re} = \frac{UR_h}{\nu}$	3.41×10^4		Width-depth ratio, w/h	4.09
Froude number, $Fr = \frac{U}{\sqrt{gh}}$	0.97		Relative boundary layer thickness, δ / h	0.80

5.3.2 SETUP FOR NUMERICAL EXPERIMENT

The setup of numerical experiment totally repeats the real experiment setup and boundary conditions. Figure 5.4 shows the situation sketch of setup for numerical simulation. The detailed information of physical constants and boundary conditions are introduced in the following text.

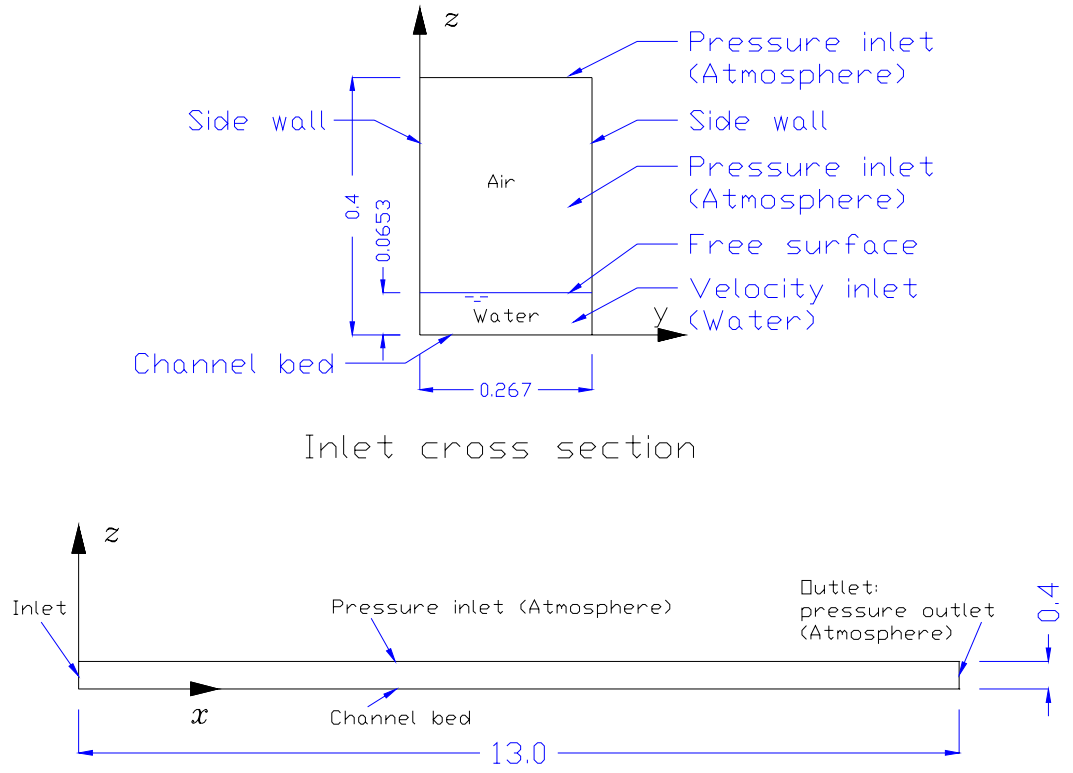

Figure 5.4 Situation sketch of numerical experiment setup (unit: m)

5.3.2.1 FLUID PROPERTIES

In FLUENT, physical properties of fluids are associated with named “materials”, and these materials are then assigned as boundary condition for zones. In this project, the water properties, which provided in the database of FLUENT, were used in all the case studies.

Water density, ρ = 998.2 kg/m^3

Water viscosity, μ = 1.003×10^{-3} Ns/m^2

Water-air Surface Tension, σ = 7.36×10^{-2} N/m

5.3.2.2 OPERATING CONDITION

a) Atmospheric pressure

Atmospheric pressure: 101325 Pa

b) Gravitational Acceleration

x-direction = $gS = 9.81\times0.0027 = 0.026487$ m/s^2 (along the slope)

y-direction = 0 m/s^2

z-direction = -9.81 m/s^2 (downwards)

c) Multiphase model

The Volume of Fluid (VOF) multiphase model was employed in the simulation of interaction between water and air in this thesis. The Geometric Reconstruction Approach was used for the calculation of face fluxes for the VOF model.

d) Turbulence model

As abovementioned in last section, Reynolds Stress Model was used in the simulation in the project. The Enhanced Wall Treatment was used for near wall treatment. All model constants were used as the default values provided in FLUENT.

e) Initial velocity

For water:

x-direction velocity = 0.772 m/s

y-direction velocity = 0 m/s

z-direction velocity = 0 m/s

For air

x-direction velocity = 0 m/s

y-direction velocity = 0 m/s

z-direction velocity = 0 m/s

Initial velocity must be large enough so that the simulation model is a turbulent flow. One way to check whether an open-channel flow is turbulent flow or not is to calculate the Reynolds number, which is defined as:

$$\mathrm{Re} = \frac{UR_h}{\nu} \tag{5.1}$$

where U is the average velocity, R_h is the hydraulic radius, ν denotes the kinematic viscosity. When Re > 500 ~ 2000, the flow is turbulent flow.

For a rectangular section in this case, $R_h = hw/(w+2h) = 0.0438$ m where w is the breadth and h is the depth. Reynolds number is equal to 33625. That is far greater than 2000 and reasonably high. Hence, the simulation flow mode is fully turbulent flow.

5.3.2.3 BOUNDARY CONDITHONS

Boundary conditions are a critical component of FLUENT simulation and it is important that they are specified appropriately. Figure 5.4 shows the details of the boundary conditions of numerical simulation setup. All the boundary conditions were set to repeat the real experiment boundary conditions.

a) Inlet

Inlet cross section was split into two components as shown in Figure 5.4. The lower part (0.267m×0. 0653m) is water velocity inlet which velocity was specified as the average velocity 0.772 m/s. The upper part is pressure inlet boundary. Its pressure is equal to the atmospheric pressure.

b) Outlet

Outlet was set as a simple pressure outlet boundary which pressure also was specified as the atmospheric pressure.

c) Top surface

Top surface was set as a pressure inlet boundary which pressure was specified as the atmospheric pressure, too.

d) Open-channel bed and side walls

The bed and side walls were set as stationary walls with the no-slip condition. Wall roughness was negligible in the studies.

e) Default interior

The default interior was the mixture of water and air. The water depth will be decided by the computation.

f) Grid and adaption

The whole domain of open channel was discretized with 200,000 hexahedron cells. The initial cell distribution sketch is shown in Figure 5.5. The shape of cells containing water are better than those containing air since this project concerns on capturing the essential feature of the water flow in open channel. The mesh between x = 8.4 m and x = 9.4 m was refined in advance because the data would be captured in the cross section of x = 9 m.

5.3.3 PATCH TEST RESULTS

The observations in Lyn's experiments were taken at a section x ≈ 9 m (Lyn, 1988). So the following data of numerical simulation also were taken at the section x = 9 m. The FLUENT computing results showed the variation of water depth was equal to zero at this

section. It means the flow has developed into uniform open-channel flow before this section.

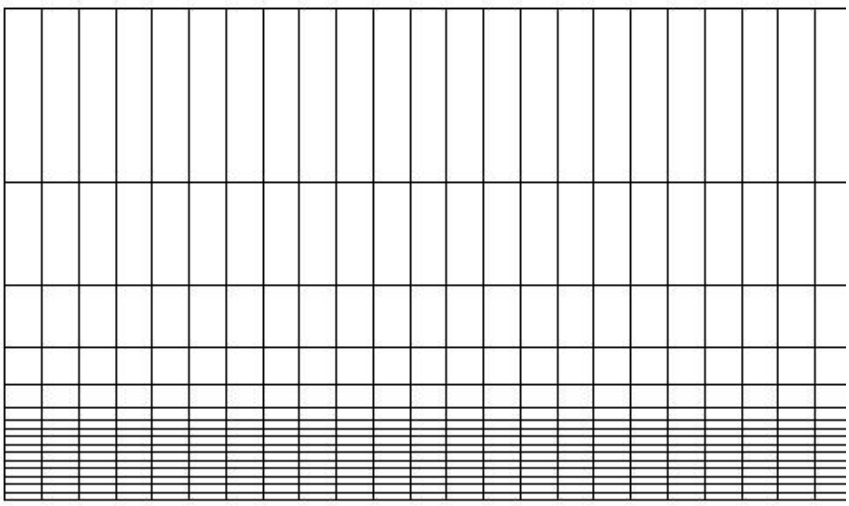

Figure 5.5 Grid sketch of part of the longitudinal section

Figures 5.6 and 5.7 depict the predicted contours of mean primary velocity and secondary flow at section x = 9 m, respectively. One can see the maximum velocity occurred under the free surface. The predicted x-wall shear stress distribution on the bed (x = 9 m) is described in Figure 5.8. These three figures show the typical characteristics of a normal uniform open-channel flow.

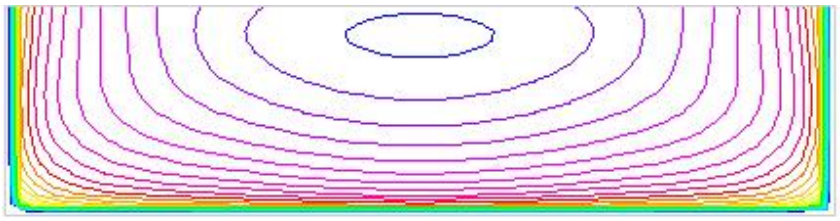

Figure 5.6 Predicted contour lines of mean primary velocity at section x = 9 m

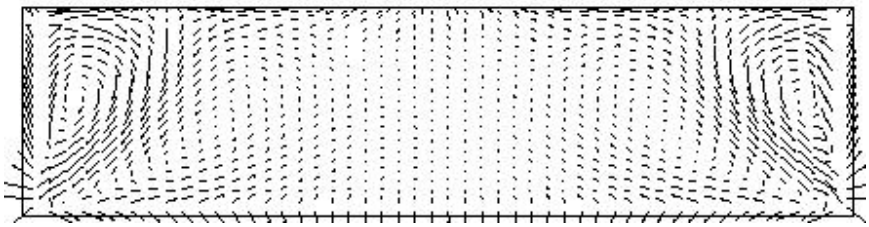

Figure 5.7 Predicted vector descriptions of secondary currents at section x = 9 m

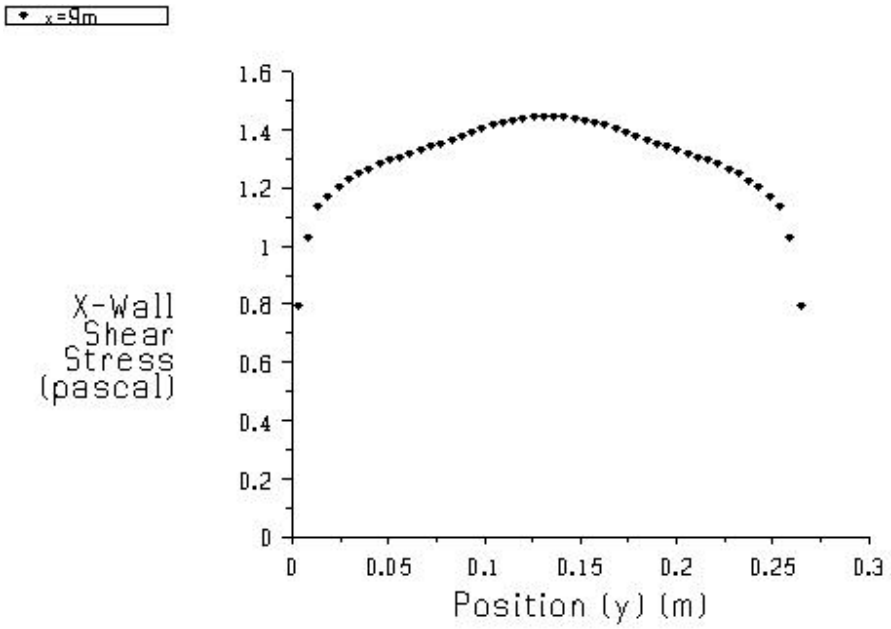

Figure 5.8 Predicted x-wall shear stress distribution at section x = 9 m (on the bed)

From Figure 5.9 it can be seen that the predicted velocity distribution for open channel flow coincides with the measured distribution. A slight deviation of the predicted distribution from the measured one can be noticed, but it is well within the scatter of the experimental points.

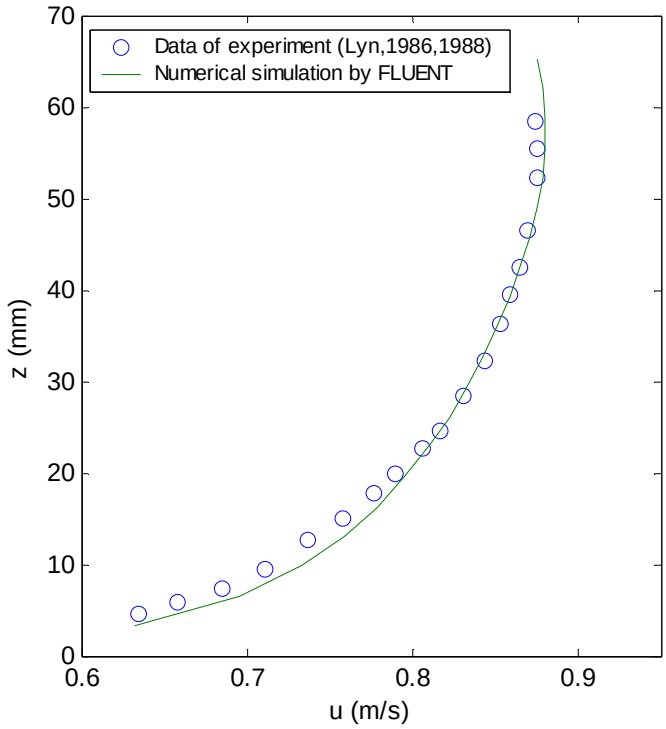

Figure 5.9 Comparison of predicted primary velocity with measurement

(centreline at x = 9 m)

The comparisons of other basic properties for open-channel flow between the prediction and measurement are listed in Table 5.3. One can see the largest difference is less than 3%. The predicted values agree with measured values very well.

Judging from the agreement between the predicted velocity (and wall shear velocity) and the measurement, it can be concluded that the numerical experiment setup and boundary conditions in FLUENT is adequate to predict the mean flow properties of turbulent open-channel flows.

Table 5.3 Comparison of basic properties between prediction and measurement

Property	Measured value	Predicted value	Relative error
(1)	(2)	(3)	[(3) – (2)]/(2)
Average velocity U (m/s)	0.772	0.749	-0.029
Maximum velocity, u_{max}, (m/s)	0.874	0.881	0.008
Depth, h (m)	0.0653	0.0673	0.030
Bed shear velocity, u_{*b} (m/s)	3.7	3.8	0.027

5.4 SUMMARY

The comparison between the predicted velocity (and wall shear velocity) and the measurement shows that the numerical simulation can be successfully conducted with appropriate setup designs and boundary conditions using FLUENT. The numerical experiment results are reasonably reliable and accurate.

CHAPTER SIX

NUMERICAL EXPERIMENTS OF DECELERATING FLOWS IN WIDE OPEN CHANNEL

6.1 INTRODUCTION

The modified log-wake law (MLWL) was developed from the turbulent flat plate boundary layers which always are regarded as two dimensional problems. It is natural to consider employing the MLWL to simulate the mean primary velocity profiles of wide open-channel (aspect ratio $w/h > 5$) flows which also are often simplified as 2D problems. In this chapter, the numerical simulations are reduced to 2D cases from 3D problems. It is reasonable to expect the guarantee of patch test conducted in Chapter 5 should be hold on in 2D fields.

The details of setup design and corresponding situations for numerical experiments are described in Section 6.2. Section 6.3 and 6.4 show the numerical experiments' results, analysis and discussion. The correlation of Π and a new pressure gradient parameter β_p

for wide open-channel flows is decided in Section 6.5. At last, Section 6.6 summarizes a brief conclusion of this chapter.

6.2 SETUP FOR NUMERICAL EXPERIMENT

The setup for numerical experiments in this chapter is similar to the setup of the patch test in Section 5.3 except the dimensions changed to two. Furthermore, in order to capture the phenomena of decelerating flows in wide open channel, some "obstacles (wall)" were set at the outlet section to produce adverse pressure gradient by increasing the flow depth. The situation sketch of setup for numerical simulations is shown in Figure 6.1.

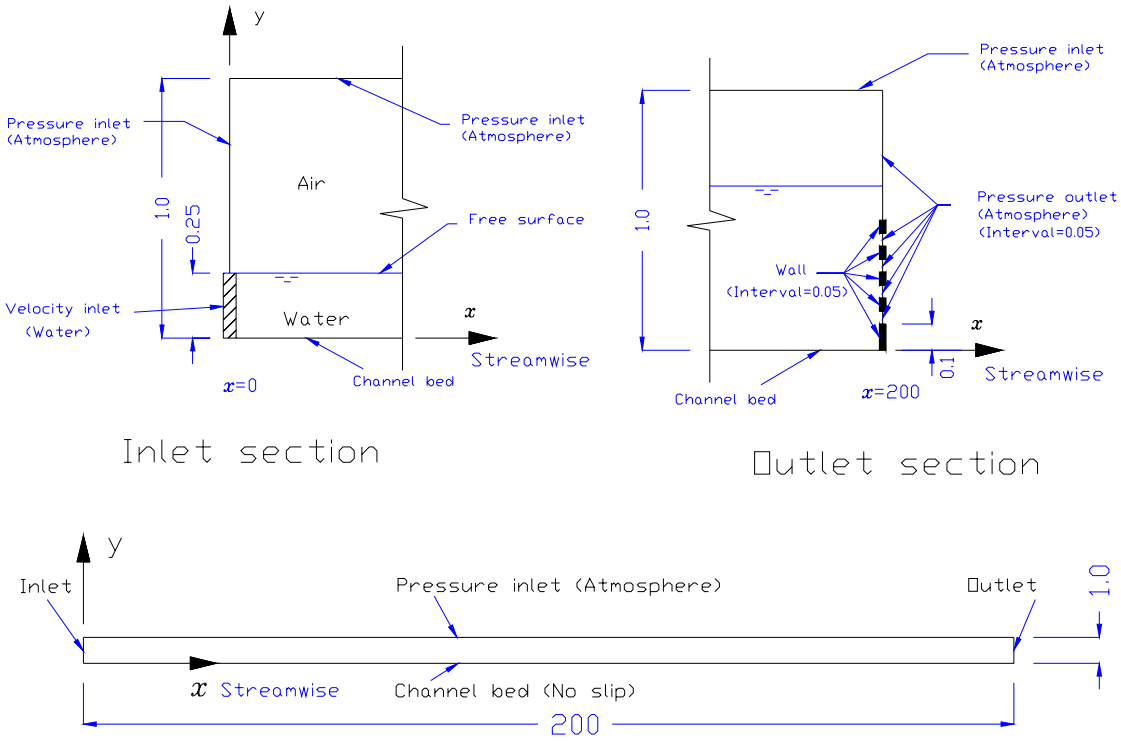

Figure 6.1 Situation sketch of numerical experiment setup (unit: m, not in proportion)

All the numerical experiments conducted in this chapter use the same setup described in Figure 6.1. Different cases would be produced by changing the operating conditions, such as gravitational acceleration in *x* direction g_x and flowrate etc. The 2D open channel is smooth with 200 m long and 1 m high. It is long enough to let the flow reach a fully-developed uniform status before the hydraulic jump which takes place because the water depth changed by the "obstacles" set at the outlet. The flowrate would be controlled to approximate an almost 0.25 m deep uniform open channel flow corresponding to different bottom slopes. The detailed information of physical constants and boundary conditions are introduced in the following text.

6.2.1.1 FLUID PROPERTIES

In this thesis, the water properties, which provided in the database of FLUENT, were used in all the case studies.

Water density, ρ = 998.2kg/m^3

Water viscosity, μ = 1.003×10^{-3} Ns/m^2

6.2.1.2 OPERATING CONDITION

a. Atmospheric pressure

Atmospheric pressure: 101325 Pa

b. Gravitational Acceleration

x-direction = $g_x = gS = 9.81S$ m/s^2 (along the slope), where S denotes the bottom slope.

y-direction = $g_y = -gtg^{-1}(S) = -9.81tg^{-1}(S)$ m/s^2 (downwards)

c. Multiphase model

The Volume of Fluid (VOF) multiphase model was employed in the simulation of interaction between water and air in this thesis. The Geometric Reconstruction Approach was used for the calculation of face fluxes for the VOF model.

d. Turbulence model

Reynolds Stress Model was used in the simulation in this thesis. The Enhanced Wall Treatment was used for near wall treatment. All model constants were used as the default values provided in FLUENT.

e. Initial velocity

For water:

x-direction velocity = U m/s, where U is the average velocity in each case.

y-direction velocity = 0 m/s

For air

x-direction velocity = 0 m/s

y-direction velocity = 0 m/s

Initial velocity must be large enough so that the simulation model is a turbulent flow. In each numerical simulation case, the average velocity U is larger than 1 m/s, the hydraulic radius is larger than 0.1 m, hence, the Reynolds number $\mathrm{Re} = \frac{UR_h}{\nu}$ should be larger than 9×10^4 >> 500 ~2000, the simulation flow mode is fully turbulent flow.

6.2.1.3 BOUNDARY CONDITHONS

The boundary conditions of numerical simulation setup are shown in Figure 6.1. The details are introduced in the following.

a. Inlet

Inlet cross section was split into two components as shown in Figure 6.1. The lower part (0.25 m) is water velocity inlet which velocity was specified as the average velocity U. The upper part is pressure inlet boundary. Its pressure is equal to the atmospheric pressure.

b. Outlet

As shown in Figure 6.1, the outlet was designed a little complex to produce the adverse pressure gradient in open-channel flow. There are five distant obstacles (wall) placed in the outlet section while other parts are pressure outlet boundary which pressure is equal to the atmospheric pressure.

c. Top surface

Top surface was set as a pressure inlet boundary which pressure was specified as the atmospheric pressure, too.

d. Open-channel bed

The bed was set as stationary wall with the no-slip condition. Wall roughness was negligible in the studies.

e. Default interior

The default interior was the mixture of water and air. The water depth will be decided by the computation.

f. Grid and adaption

The whole domain of open channel was discretized with 80,000 hexahedron cells. The initial cell distribution sketch is shown in Figure 6.2. The shape of cells containing water are better than those containing air since this project concerns on capture the essential feature of the water flow in open channel. The mesh would be refined according to the gradient of flow characteristics.

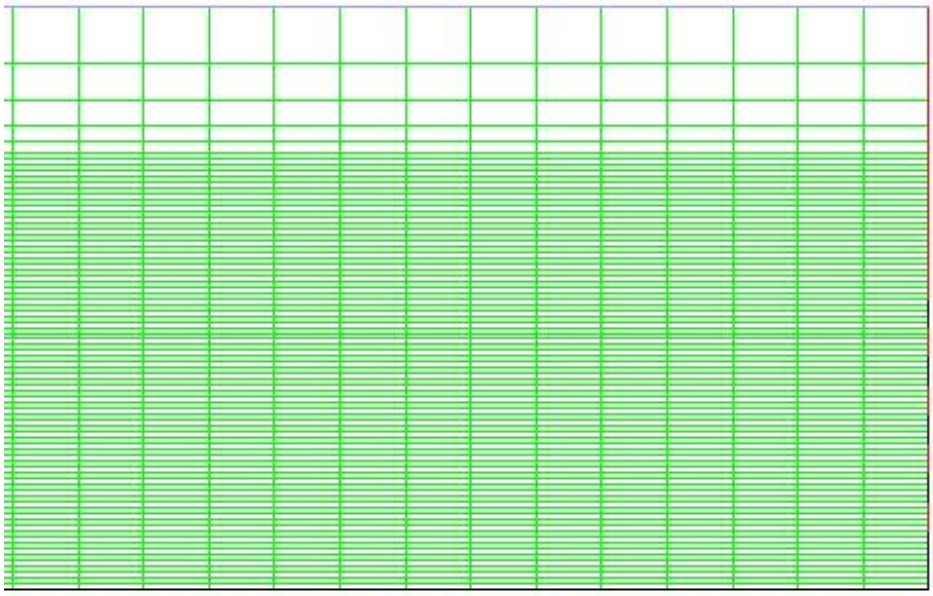

Figure 6.2 Grid sketch for part of open channel domain

6.3 NUMERICAL EXPERIMENT OF DECELERATING FLOW (S = 0.003)

The smooth flume, 200 m in length, 1 m in height; in this run, the bottom slope is 0.003. The fluid with an initial depth (h = 0.25 m) flowed into the flume, developed into a fully-developed uniform open-channel flow in the long flume before it arrived the location (about x = 145 m) where the hydraulic jump was produced by the change of water depth. Passing through the hydraulic jump, the water depth increases, the elevation of water surface also increases slowly along the flume till the outlet. Avoiding the influence of hydraulic jump and outlet, six profiles of mean velocity $u(y)$ under adverse pressure gradient (deceleration) are taken from x = 185 m to x = 190 m. For comparison, one of the mean velocity profile of uniform open-channel flow at x = 130m was obtained. The relevant hydraulic parameters of the seven profiles are summarized in Table 6.1.

Table 6.1 Summary of basic data and flow parameters (S = 0.003)

Station	1	2	3	4	5	6	7
	Uniform	APG	APG	APG	APG	APG	APG
x, (m)	130	185	186	187	188	189	190
S	0.003	0.003	0.003	0.003	0.003	0.003	0.003
q, (m^3/sm)	0.59	0.59	0.59	0.59	0.59	0.59	0.59
h, (m)	0.2466	0.5717	0.5748	0.5781	0.5816	0.5855	0.5896
δ , (m)	0.21	0.49	0.49	0.49	0.49	0.49	0.50
U, (m/s)	2.393	1.032	1.026	1.021	1.014	1.008	1.001
U_{max}, (m/s)	2.566	1.122	1.117	1.110	1.103	1.096	1.090
Re_δ	11740	18388	18319	18176	18102	17949	17876
Fr	1.53	0.44	0.43	0.43	0.42	0.42	0.42
$u_* \times 10^2$,(m/s)	8.49	3.77	3.76	3.73	3.71	3.68	3.67
κ	0.4	0.414	0.416	0.415	0.416	0.416	0.418
B	5.710	5.71	5.72	5.75	5.73	5.76	5.76
Π	0.1729	0.2591	0.2719	0.2810	0.2887	0.2962	0.3042
$\partial p / \partial x$	0. 000	32.496	32.709	32. 866	33. 203	33. 189	33. 209
$\partial p^* / \partial x$	-29.377	3.119	3.332	3.489	3.826	3.812	3.832
β	-0.053	0.081	0.088	0.095	0.106	0.108	0.110
β_h	-1.007	1.13	1.36	1.45	1.62	1.65	1.68
β_p	0	13.090	13.346	13.699	14.041	14.368	1.597

x: distance form the flume entrance to the "measuring cross –section"; S: channel bottom slope; $q=hU$: discharge per unit width; h: water depth; δ : distance from the bottom to the maximum velocity point; U: mean (depth averaged) velocity; U_{max}: maximum velocity in the profile; $\mathrm{Re}_\delta = \delta u_* / \nu$: Reynolds number; ν : kinematic viscosity; $Fr = U/\sqrt{gh}$: Froude number; g: gravitational acceleration; u_* : friction velocity; κ : van Kaman constant; B: additional constant of integration of the log law (3.23); Π : Coles' wake strength; $\partial p/\partial x = \rho g(\partial h/\partial x)$: longitudinal pressure gradient; $\partial h/\partial x$: longitudinal water depth variation; $\partial p^*/\partial x = \rho g(-S + \partial h/\partial x) = -\rho g S + \partial p/\partial x$: pressure gradient; $\beta = (\delta^*/\rho u_*^2)(\partial p^*/\partial x)$: pressure gradient parameter; $\beta_h = (h/\rho u_*^2)(\partial p^*/\partial x)$: pressure gradient parameter for flume flow; δ^*: displacement thickness; $\beta_p = (h/\rho u_*^2)(\partial p/\partial x)$: new pressure gradient parameter for flume flow.

Since the free stream flow disappears in fully developed open-channel flows, the boundary conditions for open-channel flows are somewhat differ from those for flat plate boundary layers. Hence, the coefficients in log law, log-wake law and modified log-wake law, such as von Karman constant κ and additional constant B, are possibly different in two situations. For open-channel flows in this study, the value of κ and B can be determined based on a parameter curve fit of log law (2.1) to the data of velocity profile in the region $0.02 \le y/\delta \le 0.15$, because all open-channel flow should strictly obey the log law (2.1) in the inner region ($0.02 \le y/\delta \le 0.2$). The determined κ and B are already listed in Table 6.1. Both κ and B are functions in terms of $\mathrm{Re}_\delta = \delta u_* / \nu$ which were interpreted in Chapter 3. But the range of Reynolds number gained in this study

($17870 < \mathrm{Re}_\delta = \delta u_* / \nu < 18390$) is too short to carry out the functions. In this short range of Reynolds number, they are almost constants, the mean of each coefficient could be gotten as following:

$$\kappa = 0.415 \tag{6.1}$$

$$B = 5.7 \tag{6.2}$$

They are slightly different from those used in describing flat plate boundary layers.

Let's return to concern on the modified log-wake law (MLWL). The comparison of predicted values of MLWL (4.1) with the numerical experimental data is shown in Figure 6.3. A log law with the values of coefficients (κ and B) listed in Table 6.1 also is drawn in Figure 6.3. One can see the MLWL agrees with the numerical experimental date excellently.

As shown in Table 6.1 and Figure 6.3, the maximum velocities occur below the free surface. This phenomenon obviously results from the damping effects of free surface while the influence of side walls is not considered in 2D open-channel problems. However, the MLWL could predict the velocity profiles in the region above the point which the maximum velocity occurs well. This is a main distinct advantage of the MLWL. On the contrary, log law is false to predict the outer region and completely can not describe the region above the maximum velocity.

Similar in Chapter 4, the parameter Π gained in the curve fit process for each velocity profile is shown in Table 6.1. The correlation of Coles' wake strength Π with pressure gradient parameter β will be treated with other numerical data in Section 6.5.

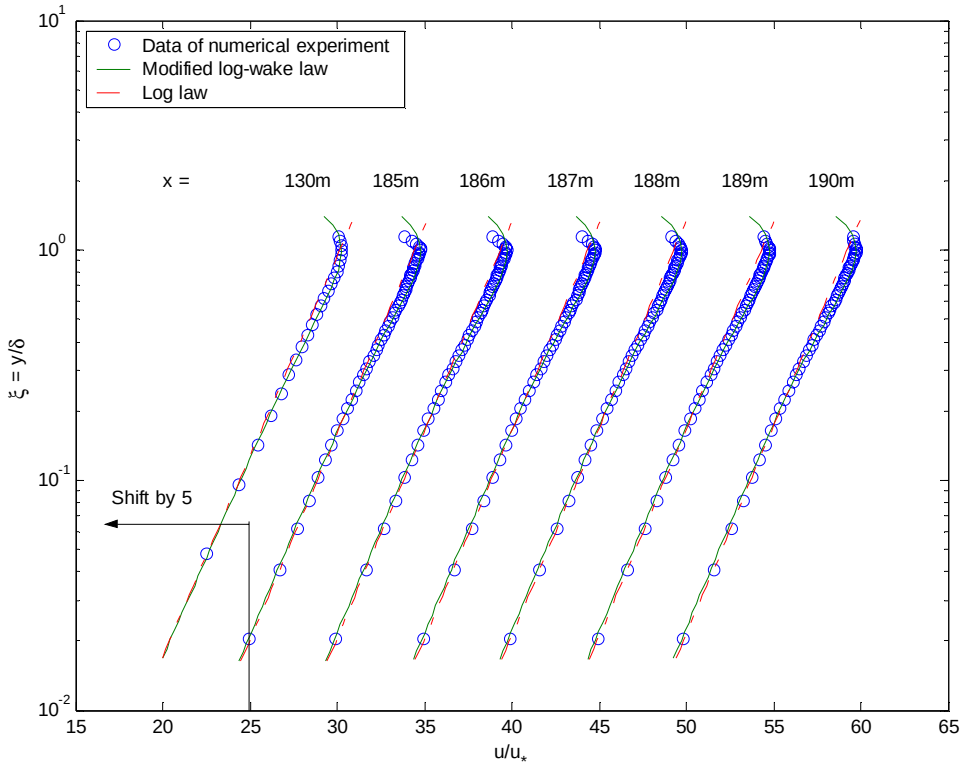

Figure 6.3 Comparison of the modified log-wake law with numerical experiments (S=0.003)

6.4 NUMERICAL EXPERIMENT OF DECELERATING FLOW (S = 0.00275)

The smooth flume, also 200 m in length, 1 m in height; in this run, the bottom slope is 0.00275. The fluid with an initial depth (h = 0.25 m) flowed into the flume, developed into a fully-developed uniform open-channel flow in the long flume before it arrived the

location (about x = 140 m) where the hydraulic jump was produced by the change of water depth. Passing through the hydraulic jump, the water depth increases, the elevation of water surface also increases slowly along the flume till the outlet. Avoiding the influence of hydraulic jump and outlet, five profiles of mean velocity $u(y)$ under adverse pressure gradient (deceleration) are taken from x = 180 m to x = 185 m. For comparison, one of the mean velocity profile of uniform open-channel flow at x = 120m was obtained. The relevant hydraulic parameters of the six profiles are summarized in Table 6.2.

The determined κ and B are listed in Table 6.2. They are coincident with (6.1) and (6.2), respectively.

The comparison of predicted values of MLWL (4.1) with the numerical experimental data is shown in Figure 6.4. One can see the MLWL agrees with the numerical experimental data excellently. Furthermore, the MLWL could predict the velocity profiles in the region above the point which the maximum velocity occurs well. The distinct advantage of the MLWL does work well. On the contrary, log law is again false to predict velocities in the outer region and completely can not describe the region above the maximum velocity.

The parameter Π gained in the curve fit process for each velocity profile is shown in Table 6.2. The correlation of Coles' wake strength Π with pressure gradient parameter β will be treated with other numerical data in Section 6.5.

Table 6.2 Summary of basic data and flow parameters (S = 0.00275)

Station	1	2	3	4	5	6
	Uniform	APG	APG	APG	APG	APG
x (m)	120	180	181	182	183	184
S	0.00275	0.00275	0.00275	0.00275	0.00275	0.00275
q, (m^3/sm)	0.568	0.568	0.568	0.568	0.568	0.568
h, (m)	0.2472	0.5483	0.5513	0.5546	0.5582	0.5623
δ , (m)	0.21	0.48	0.48	0.48	0.48	0.48
U, (m/s)	2.298	1.036	1.030	1.024	1.018	1.010
U_{max}, (m/s)	2.452	1.113	1.106	1.100	1.094	1.087
Re_δ	17021	17994	17863	17793	17659	17586
Fr	1.48	0.45	0.44	0.44	0.43	0.43
$u_* \times 10^2$,(m/s)	8.14	3.77	3.74	3.72	3.70	3.68
κ	0.4	0.414	0.414	0.415	0.414	0.415
B	5.71	5.69	5.71	5.70	5.73	5.72
Π	0.1730	0.2268	0.2342	0.2401	0.2464	0.2538
$\partial p / \partial x$	0. 000	29.576	30. 006	30. 200	30. 290	30. 555
$\partial p^* / \partial x$	−27. 104	2. 648	3. 077	3. 271	3. 362	3. 626
β	-0.053	0.066	0.078	0.084	0.088	0.097
β_h	-1.012	1.03	1.22	1.31	1.38	1.51
β_p	0	11.518	11.920	12.163	12.467	12.774

Where the meaning of each term is the same as in Table 6.1.

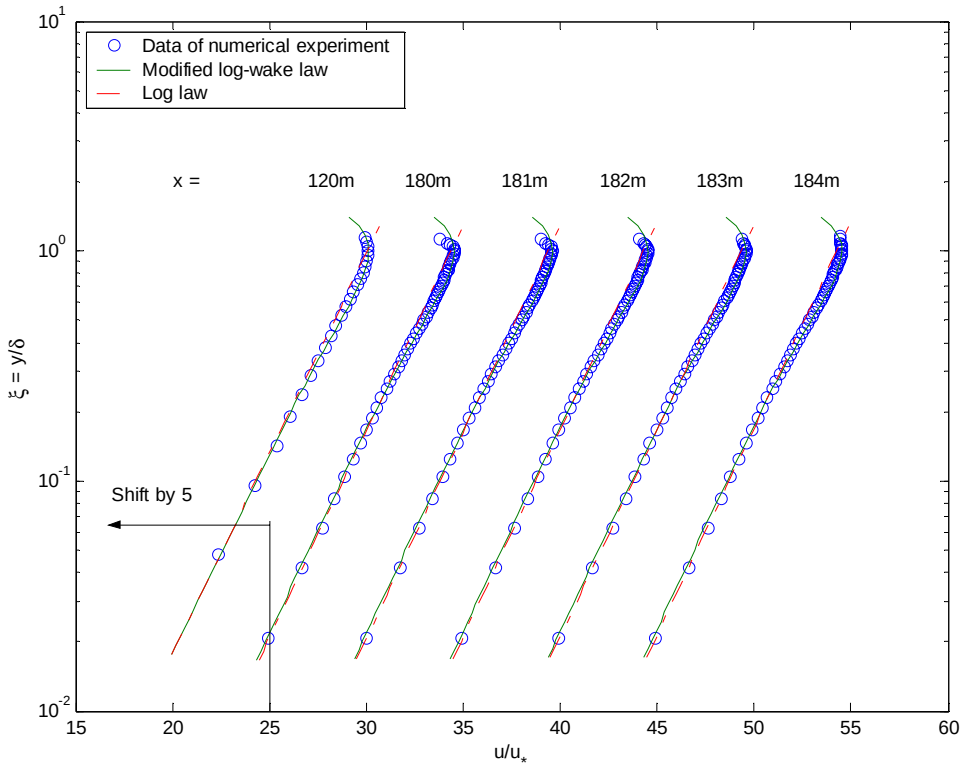

Figure 6.4 Comparison of the modified log-wake law with numerical experiments (S=0.00275)

6.5 CORRELATION OF Π WITH β

As previously mentioned, the Coles' wake strength Π reflects the effects of pressure gradient on boundary layer and open-channel flow velocity distribution. The intensity of pressure gradient is represented by the pressure gradient parameters β, β_h and β_p. A relationship of Π and pressure gradients could be carried out to predict the value of Π when a boundary layer is measured. Based on the log-wake law (2.4), Kironoto and Graf (1995) summed up a formula to express the correlation of Π with β in wide open

channel (2.7). Similarly, a third-order polynomial is employed to describe the correlation of Π with β based on the modified log-wake law (2.5).

In section 6.3 and 6.4, a value of Π corresponding to each β were gained and presented in Table 6.1 and 6.2 for each velocity profile. Figure 6.5 shows that their relationship varies with the bottom slope of open channel. The two series numerical data are not consistent with each other. This phenomenon implies that the Clauser pressure gradient $\beta = \left(\delta^* / \rho u_*^2\right)\left(\partial p^* / \partial x\right)$, which involves the bottom slope in its definition, is not appropriate to reflect the effect of pressure gradient for open-channel flows.

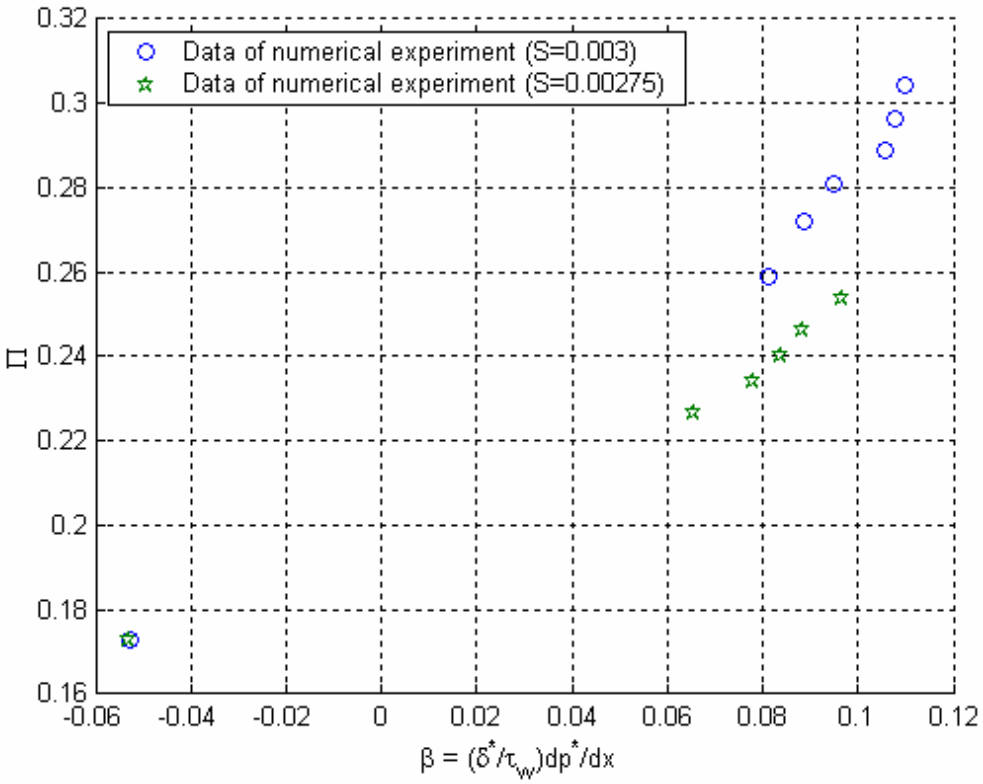

Figure 6.5 Coles wake strength Π against Clauser pressure gradient parameter β

Similarly, in section 6.3 and 6.4, a value of Π corresponding to each β_h was gained and presented in Table 6.1 and 6.2 for each velocity profile. Figure 6.6 also shows that the pressure gradient $\beta_h = \left(h/\rho u_*^2\right)\left(\partial p^*/\partial x\right)$, which involves the bottom slope in its definition, is not appropriate to reflect the effect of pressure gradient of open-channel flows.

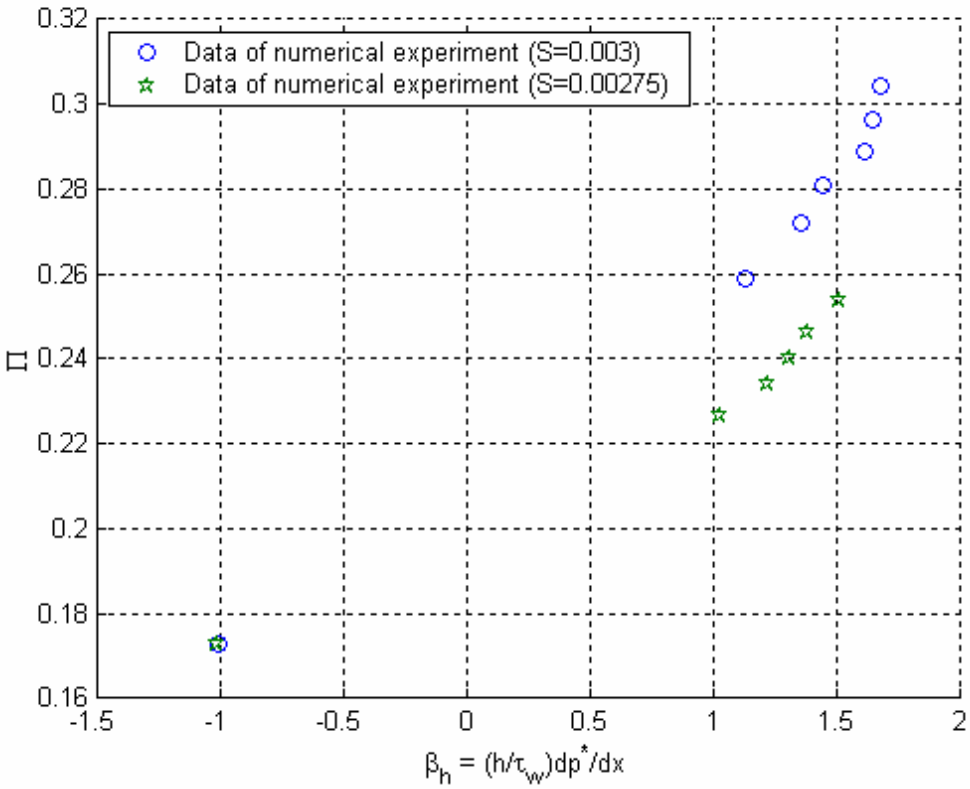

Figure 6.6 Coles wake strength Π against pressure gradient parameter β_h

On the other hand, the values of new pressure gradient $\beta_p = \left(h/\rho u_*^2\right)\left(\partial p/\partial x\right)$, in which the open-channel bottom slope is dropped in its definition, were also list in Table 6.1 and 6.2. The correlation of Π with β_p is described in Figure 6.7. One can see that the two

series of numerical data agree with each other very well. A curve fitting reveals the relationship of Π with β_p can express as

$$\Pi=5.1\times10^{-5}\beta_p^{\,3}-1.5\times10^{-4}\beta_p^{\,2}+3.5\times10^{-5}\beta_p+0.173 \tag{6.3}$$

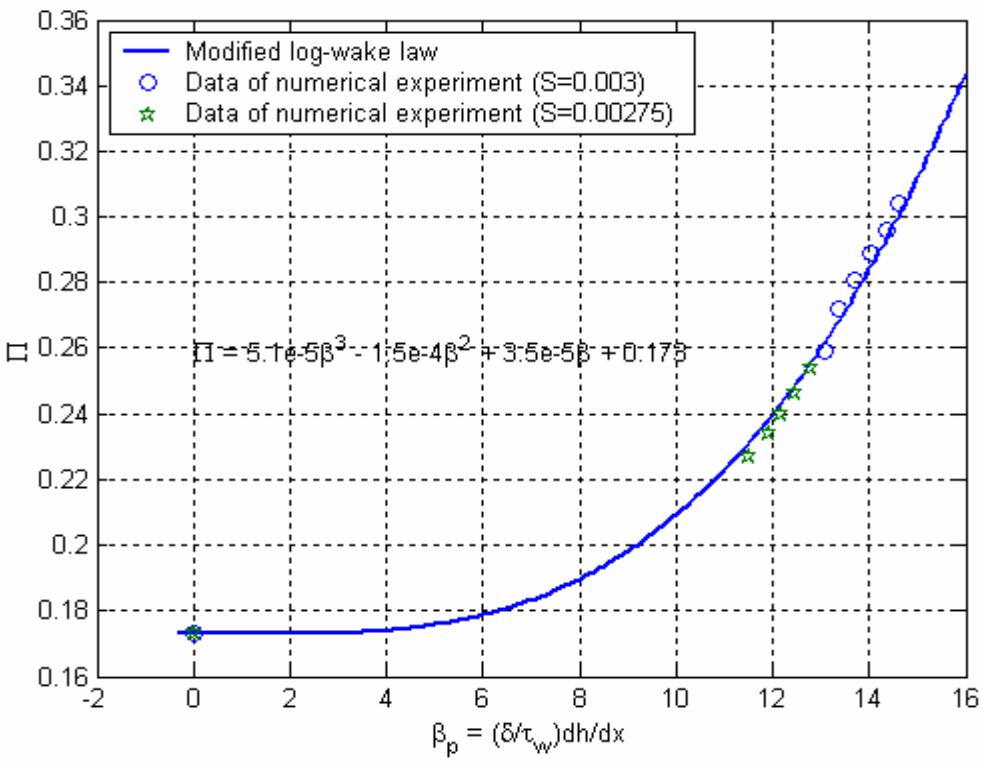

Figure 6.7 Coles wake strength Π against pressure gradient parameter β_p

6.6 SUMMARY

All of the numerical experimental data agree with MLWL quite well. The MLWL is valid for uniform or decelerating turbulent flows in wide open channel. The following conclusions can be summarized:

a) The basic structure of the MLWL is correct for decelerating open-channel flows;

b) The MLWL not only can predictt the velocity profile under the maximum velocity, but also can simulate the above region till the free surface;

c) The MLWL tends to a straight line in a semilog plot in the overlap region and then concides with the logarithmic law;

d) The zero velocity gradient at the boundary layer edge can be clearly seen from all profiles in Figures 6.3 and 6.4 which imply that the boundary correction is necessary;

e) A new pressure gradient parameter $\beta_p = \left(h / \rho u_*^2\right)\left(\partial p / \partial x\right)$, which is more appropriate to reflect the effects of pressure gradient in open channel, is first introduced in this study;

f) Based on MLWL, the Coles' wake strength Π can be predicted by (6.3).

CHAPTER SEVEN

CONCLUSIONS AND RECOMMENDATIONS

7.1 CONCLUSIONS

1) The basic structure of modified log-wake is correct. Velocity profiles of nonzero-pressure gradient flat plate turbulent boundary layers and wide open channel turbulent flows can be described by the modified log-wake law, i.e.

$$\frac{u}{u_*} = \frac{1}{\kappa}\ln\frac{yu_*}{\nu} + B + \frac{2\Pi}{\kappa}\sin^2\frac{\pi\xi}{2} - \frac{\xi^3}{3\kappa} \tag{3.36}$$

or its defect form

$$\frac{U-u}{u_*} = \frac{1}{\kappa}\left(\ln\xi - 2\Pi\cos^2\frac{\pi\xi}{2} + \frac{1-\xi^3}{3}\right) \tag{3.38}$$

in which $\Pi = \Pi_0 + \Pi_p$. Π_0 is a constant developed from ZPG boundary layers. Π_p represents the effects of pressure gradient in NPG boundary layers and changes with different pressure gradient.

2) Both κ and B are functions in terms of Reynolds number. For large Reynolds number conditions, κ keeps as a constant, B should change with Reynolds number slowly.

3) In strict boundary layers, for large Reynolds number, κ = 0.4. The value of a Π can be determined by (4.4a) with the measured Clauser pressure gradient parameter β:

$$\Pi = -0.0105\beta^2 + 0.535\beta + 0.40 \tag{4.4a}$$

4) Deceleration flows in widely open channel, around the range of Reynolds number in this study, κ = 0.415 *and* B = 5.71, both coefficient could be regarded as constants. The value of a Π can be determined by (6.3) with the measured pressure gradient parameter $\beta_p = \left(h/\rho u_*^2\right)\left(\partial p/\partial x\right)$

$$\Pi = 5.1\times10^{-5}\beta_p^{\,3} - 1.5\times10^{-4}\beta_p^{\,2} + 3.5\times10^{-5}\beta_p + 0.173 \tag{6.3}$$

5) The zero velocity gradient at the boundary layer edge can be clearly seen from all profiles in this thesis which imply that the boundary correction is necessary.

6) For open-channel flow, the MLWL not only can predictt the velocity profile in the region under the maximum velocity, but also can simulate the above region till the free surface.

7.2 RECOMMENDATIONS

Information about nonuniform open-channel flows are seldom and difficult to find. More extensive investigations may be worth to performed to construct a systematic knowledge of nonuniform open-channel flows

Application of modified log-wake law in hydraulic engineering is immediately recommended.

REFERENCES

1. Ayala, A., White, B. R., Kim, D. S., and Bagheri, N. Turbulent Transport Characteristics in a Low-Speed Boundary Layer Subjected to Adverse Pressure. In Proc. 36th Heat Transfer and Fluid Mechanics Institute, 1999, California State University, Sacramento. pp.1-13.
2. Barenblatt, G. I., Chorin, A. J. and Prostokshin, V. M. Self-Similar Intermediate Structures in Turbulent Boundary Layers at Large Reynolds Numbers. J. Fluid Mech., 410, pp.263-283. 2000.
3. Cardoso, A. H., Graf, W. H. and Gust, G. Uniform Flow in Smooth Open-Channel. J. Hydr. Res., IAHR, 27(5), pp.603-616. 1989.
4. Cardoso, A. H., Graf, W. H. and Gust, G. Steady Gradually Accelerating Flow in a Smooth Open Channel. J. Hydr. Res., IAHR, 29 (4). pp.525-543. 1991.
5. Clauser, F. H. Turbulent Boundary Layers in Adverse Pressure Gradients. J. Aero. Sci., 21, pp.21-108. 1954.
6. Clauser, F. H. The Turbulent Boundary Layer. Advances Appl. Mech., 4. pp.1-51. 1956.
7. Cokljat, D. and Younis, B. A. Second-Order Closure Study of Open-Channel Flows. J. Hydr. Engrg. ASCE. 121(2). pp.94-107. 1995.
8. Coleman, N. L. Velocity Profiles with Suspended Sediment. J. Hydr. Res., IAHR, 19(3), pp.211-229. 1981.
9. Coleman, N. L. Effects of Suspended Sediment on the Open-Channel Velocity Distribution. Water Resources Research, AGU, 22(10), pp.1377-1384. 1986.
10. Coles, D. E. The Law of the Wake in the Turbulent Boundary Layer. J. Fluid Mech.,

1, pp.191-226. 1956.

11. Coles, D. E. The Young Person's Guide to the Data. Proc. Computation of Turbulent Boundary Layers - 1968 AFOSR-IFP-STANFORD CONFERENCE, 2. pp.1-19. 1969.
12. Das, D. K. A Numerical Study of Turbulent Separated Flows. Amer. Soc. Mech. Engineers Forum on Turbulent Flows. FED 51. pp.85-90. 1987.
13. Fernholz, H. H. and Finley, P. J. The Incompressible Zero-Pressure-Gradient Turbulent Boundary Layer: An Assessment of the Data." Prog. Aerospace Sci., Pergamon. 32. pp.245-311. 1996.
14. Graf W. H. and Altinaker, M. S. Hydrodynamique Fluviale; Tome 1. Presses Polytechniques et Universitaires Romandes, Lausanne. 1993.
15. Guo, J. Turbulent Velocity Profiles in Clear Water and Sediment-Laden Flows. Ph.D Thesis, Colorado State University, Fort Collins, CO. 1998.
16. Guo, J. and Julien, P. Y. Modified Log-Wake Law in Smooth Rectangular Open-Channels. In Proc. 13th IAHR-APD Congress, August 2002, Singapore. Vol. 1, pp.87-99.
17. Guo, J., Julien, P. Y. and Meroney, R. N. Modified Log-Wake Law for Zero-Pressure-Gradient Turbulent Boundary Layers. In Proc. International Conference on Port and Maritime R & D and Technology, September 2003, Singapore. Vol. 1, pp.125-141.
18. Guo, J. and Julien, P. Y. Modified Log-Wake Law for Turbulent Flow in Smooth Pipes. J. Hydraulic Research, IAHR, 41(5), pp493-501. 2003.
19. Herring, H. J. and Norbury, J. F. Some Experiments on Equilibrium Boundary Layers in Favorable Pressure Gradients. J. Fluid Mech., 27. pp541-549. 1967.
20. Hinze, J. O. Turbulence. 2nd Ed., McGraw-Hill. 790p. 1975.

21. Keulegan, G. H. Laws of Turbulent Flow in Open Channels. J. Res. Nat. Bureau Stand., U. S. Dept. of Commerce, 21. pp.707-741. 1938.
22. Kirkgoz, S. Turbulent Velocity Profiles for Smooth and Rough Open-Channel Flow. J. Hydr. Engrg., ASCE, 115(11), pp.1543-1561. 1989.
23. Kironoto, B. A. Turbulence Characteristics of Uniform and Non-Uniform, Rough Open-Channel Flow. Ph.D Thesis, Ecole Polytechnique Federale. 1992.
24. Kironoto, B. A. and Graf, W. H. Turbulence Characteristics in Rough Uniform Open-Channel Flow. Proc Instn Civ. Engrs Wat. Marit. & Energy, 106(12), pp.333-344. 1994.
25. Kironoto, B. A. and Graf, W. H. Turbulence Characteristics in Rough Non-Uniform Open-Channel Flow. Proc Instn Civ. Engrs Wat. Marit. & Energy, 112(12), pp.336-348. 1995.
26. Laufer, J. The Structure of Turbulence in Fully Developed Pipe Flow. Report 1174, National Advisory Committee of Aeronautics, Washington, D. C. 1954
27. Lemmin, U. and Rolland, T. Acoustic Velocity Profile for Laboratory and Field Studies. J. Hydr. Engrg., ASCE, 123(12), pp.1089-1098. 1997.
28. Lyn, D. A. Turbulence and Turbulent Transport in Sediment-Laden Open-Channel Flows. W. M.Keck Laboratory of Hydraulics and Water Resources, California Institute of Technology, Pasadena, CA. 1986.
29. Lyn, D. A. A Similarity Approach to Turbulent Sediment-Laden Flows in Open-Channels. J. Fluid Mechanics. 193. pp.1-26. 1988.
30. Lyn, D. A. Regression Residuals and Mean Profiles in Uniform Open-Channel Flows. J. Hydr. Engrg., ASCE, 126(1), pp.24-32. 2000.
31. Marusic, I. and Perry, A. E. A Wall-Wake Model for the Turbulence Structure of Boundary Layers, Part 2. Further Experimental support. J. Fluid Mech. 298. pp.389-

407. 1995.

32. Nagano, Y., Tsuji, T. and Houra, T. Structure of Turbulent Boundary Layer Subjected to Adverse Pressure Gradient. Int. J. Heat Fluid Flow, 19. pp.563-572. 1998.
33. Nagano, Y., Tagawa, M. and Tsuji, T. Effects of Adverse Pressure Gradients on Mean Flows and Turbulence Statistics in a Boundary Layer. In Turbulent Shear Flows 8, ed by Durst, F., Friedrich, R., Launder, B. E., Schmidt, F. W., Schumann, U., Whitelaw, J. H., pp.7-21. Berlin: Springer. 1992.
34. Nezu, I. and Nakagawa, H. Turbulence in Open-Channel Flows. IAHR Monograph Series, A.A. Balkema Publishers, 281p. 1993.
35. Nezu, I, and Rodi, W. A. Open-Channel Flow Measurements with a Laser Doppler Anemometer. J. Hydr. Eng., ASCE, 112(5), pp.335-355. 1986.
36. Perry, A. E. and Marusic, I. A Wall-Wake Model for the Turbulence Structure of Boundary Layers, Part 1. Extension of the attached eddy hypothesis. J. Fluid Mech. 298. pp.361-388. 1995.
37. Schlichting, H. and Gersten, K. Boundary-layer Theory. McGraw- Hill, 791p. 2000.
38. Skare, P. E. and Krogstad, P. A. A Turbulent Equilibrium Boundary Layer Near Separation. J. Fluid Mech. 272. pp.319-348. 1994.
39. Samuel, A. E. and Jouber, P. N. A Boundary Layer Developing in a Increasingly Adverse Pressure Gradient. J. Fluid Mech. 66. pp.481-505. 1974.
40. Termes A. Water Movement Over a Horizontal Bed and Solitary Sand Dune. Report R/1984/H/8, Dept. of Civil Engrg., Delft University. 1984.
41. Tominaga, A. and Nezu, I. Velocity Profiles in Steep Open-Channel Flows. J. Hydr. Engrg., ASCE, 118(1). Pp.73-90. 1992.
42. Tsujimoto, T., Saito A. and Nitta K. Open-Channel Flow With Spatial Acceleration

or Deceleration. KHL Progress Report. Hydr. Lab., Kanazawa University. 1990.

43. Wang, F. M., Chew, Y. T., Khoo, B. C. and Yeo, K. S. Computation of Turbulent Flow in a Square Duct: Aspects of the Secondary Flow and Its Origin. Computer Fluids. 23(1). pp.157-176. 1994.
44. White, F. M. Viscous Fluid Flow. McGraw-Hill, 614p. 1991.